UNIVERSIDADE D
COIMBRA

Nuno Gonçalo Torres Cavaleiro

EFFECT OF CRACK FLANK HOLES ON FATIGUE CRACK GROWTH

Dissertação no âmbito do Mestrado Integrado em Engenharia Mecânica, na especialidade de Produção e Projeto orientada pelo Professor Doutor Diogo Mariano Simões Neto e pelo Mestre Edmundo Rafael de Andrade Sérgio e apresentada ao Departamento de Engenharia Mecânica da Faculdade de Ciências e Tecnologia da Universidade de Coimbra

Julho de 2022

1 2 9 0

FACULDADE DE CIÊNCIAS E TECNOLOGIA
UNIVERSIDADE D COIMBRA

Effect of crack flank holes on fatigue crack growth

A dissertation submitted in partial fulfilment of the requirements for the degree of Master in Mechanical Engineering in the speciality of Manufacturing and Design

Efeito de furos nos flancos da fenda na propagação de fendas por fadiga

Author

Nuno Gonçalo Torres Cavaleiro

Advisors

Professor Doutor Diogo Mariano Simões Neto

Mestre Edmundo Rafael de Andrade Sérgio

Committee

Chair	**Professor Doutor José António Martins Ferreira** **Professor Catedrático da Universidade de Coimbra**
Member	**Professor Doutor Joel Alexandre da Silva Jesus** **Professor Adjunto do Instituto Superior de Engenharia de Lisboa**
Advisor	**Professor Doutor Diogo Mariano Simões Neto** **Professor Auxiliar da Universidade de Coimbra**

Coimbra, July, 2022

Aos meus pais.

ACKNOWLEDGEMENTS

I would like to express my deepest appreciation to everyone that has helped me throughout the making of this dissertation and, of course, my academic path at the University of Coimbra.

To my advisors, Professor Diogo Mariano Simões Neto, and Mestre Edmundo Sérgio, for all the knowledge, patience, availability, and support along the way.

To Professor Fernando Antunes, for all the insights and valuable knowledge, availability, and encouragement.

To the Technology Group of Mechanical Engineering Department for the availability of the finite element program, DD3IMP.

To my parents and grandparents, who always stand by my side and give me the most precious advice. Without them, this wouldn't have been possible.

To my girlfriend, for all the patience and advice, and for always believing in me. This path is not always easy, and her help and shelter got me through the hardest times.

To my childhood friends that all my life have been by my side.

To the best friends that Coimbra gave me, Kévin Oliveira, Tiago Galiza, Simão Antunes, Diogo Castanhas, Pedro Lourenço, João Pina, Joana Almeida, Diogo Fonseca, Francisco Castanheira, Frederico Bravo, Rute Vasconcelos, João Antunes, Sara Gonçalves, Dalila Gomes, Carlos Santos, Gonçalo Pimentel, Ana Pastilha, José Santana, Inês Barreto, for all the amazing times we spent together. Friends I certainly will take with me for life.

This research work was sponsored by national funds from the Portuguese Foundation for Science and Technology (FCT) under the project with reference PTDC/EME-EME/31657/2017 and by European Regional Development Fund (ERDF) through the Portugal 2020 program (PT2020) and the Centro 2020 Regional Operational Programme (CENTRO-01-0145-FEDER-031657).

Abstract

Most mechanical components are subjected to cyclic loads, which may induce fatigue failure. It is estimated that 80 to 90% of failures in components working at environment temperature are connected to fatigue. This way, it is of utter importance to accurately design components and machines according to a given useful life. This life will be highly influenced by material, geometry, loading, environment, and temperature conditions. Therefore, it is important to find a way of determining parameters such as fatigue crack growth rate (FCGR) and crack tip opening displacement (CTOD). Both these parameters can be estimated through experimental testing, but it requires a lot of time and effort, as well as proper equipment. Anyway, the experimental results are a main source of fatigue data because they are extremely reliable. Numerical modelling appears as an alternative approach, mitigating some of the experimental constraints and allowing to predict the fatigue life in a faster and easier way.

The main objective of this thesis is to evaluate the effect of crack flank holes on FCG. A numerical approach, based on the cumulative plastic deformation at the crack tip, was employed to study the effects of lateral holes to the crack flanks. Accordingly, distinct diameters and hole positionings were addressed. A CTOD study was performed so that the mechanisms behind FCG can be better understood. CT specimens were modelled using the 2024-T351 aluminium alloy. Five geometries were considered to study the effect of the diameter and positioning of crack flank holes. The comparison between numerical and experimental results, due to material availability at the laboratory, will be performed for the 2050 alloy, where only one geometry with two pairs of holes drilled was considered.

The results show that drilled holes behind the crack tip are beneficial, reducing fatigue crack growth rates. In fact, larger holes, closer to the crack, shown to be the best solution. However, the overall number of cycles needed to achieve the final studied crack length is higher when no hole is drilled, indicating that having the hole from the start is not beneficial. It is important to note that crack closure in drilled specimens has shown no significant effect on FCG rates, therefore not explaining the effect of geometry in this parameter, since non-drilled specimens presented higher crack closure levels. Experimental work is now

underway. Accordingly, this will allow to compare numerical and experimental results in the case of a 2050-T8 aluminium alloy with pairs of drilled holes.

Keywords: Fatigue crack growth, finite element analysis, hole drilling, crack retardation, crack closure.

Resumo

A maioria dos componentes mecânicos estão sujeitos a cargas cíclicas que são responsáveis pelas suas falhas por fadiga. Estima-se que entre 80 e 90% das falhas em componentes mecânicos em serviço à temperatura ambiente sejam originadas por fadiga. Assim, é de extrema importância o rigoroso dimensionamento dos componentes de acordo com uma determinada vida útil. Esta vida irá ser altamente influenciada pelo material constituinte do componente, a sua geometria, o carregamento e as condições do ambiente e de temperatura. É, portanto, importante encontrar um modo de determinar parâmetros como a velocidade de propagação da fenda e o CTOD (*crack tip opening displacement*). Ambos estes parâmetros podem ser estimados por via experimental, mas este é um processo que requer bastante tempo e esforço, bem como equipamentos adequados. Porque a fadiga depende de vários fatores, a abordagem experimental debruça-se maioritariamente sobre as propriedades mecânicas dos materiais. Ainda assim, os resultados experimentais são a principal fonte de informação sobre fadiga porque são altamente confiáveis. Para mitigar todos estes constrangimentos, uma segunda abordagem através de modelação numérica facilita imenso a previsão da vida à fadiga, fazendo-o de forma mais rápida e cómoda.

O objetivo principal desta tese é comparar os resultados numéricos com os resultados experimentais, usando diferentes diâmetros e posicionamentos através da deformação plástica acumulada na extremidade da fenda. Um estudo do CTOD foi efetuado para compreender melhor os mecanismos por detrás da propagação de fendas por fadiga. Provetes CT foram modelados com recurso a duas ligas de alumínio, nomeadamente a AA2024-T351 e a AA2050-T8. Para a liga AA2024-T351, foram consideradas cinco geometrias de modo a estudar o efeito do diâmetro e posicionamento dos furos nos flancos da fenda. A comparação de resultados numéricos com experimentais, por motivos de disponibilidade de materiais no laboratório, irá ser realizada para a liga AA2050-T8, onde apenas uma geometria com dois pares de furos foi considerada.

Os resultados mostram que a presença de furos atrás da extremidade da fenda promove uma redução nas velocidades de propagação da fenda. De facto, furos de tamanho superior mais próximos da fenda são a melhor solução para diminuir a velocidade de propagação. No entanto, o número total de ciclos de carga necessários para atingir o comprimento de fenda

final estudado é superior quando nenhum furo está presente, indicando que a furação desde o início não é benéfica. É importante salientar que o efeito do fecho de fenda em provetes com furo não mostrou efeito significativo na velocidade de propagação, não explicando o efeito da geometria neste parâmetro, sendo que provetes sem furos apresentavam valores de fecho de fenda superiores.

Palavras-chave: Crescimento de fendas de fadiga, análise de elementos finitos, furação, retardação de fenda, fecho de fenda.

Contents

LIST OF FIGURES

LIST OF TABLES

LIST OF SIMBOLS AND ACRONYMS/ABBREVIATIONS

List of Symbols

a – Crack length

a_0 – Initial crack length

C, m – Constants for the Paris-Erdogan Law

C_X – Armstrong & Frederick kinematic law parameter

C_Y – Voce isotropic law parameter

D – Hole diameter

E – Young Modulus

da/dN – Fatigue crack growth rate

$F(\boldsymbol{A})$ – Cost function

F_{max} – Maximum load

F_{min} – Minimum load

F_{open} – Crack opening load

K – Stress intensity factor

K_{IC} – Fracture toughness

K_F – Opening mode stress intensity factor

K_{max} – Maximum stress intensity factor

K_{min} – Minimum stress intensity factor

K_R – Retardation stress intensity factor

K_S – Shear stress intensity factor

n – Swift law parameter

R – Stress ratio

t^* – Pseudo-time

U^* – Crack closure level

V – Vertical hole position

$\boldsymbol{X}'$ – Deviatoric component of the Cauchy stress tensor

X_{Sat} – Kinematic saturation stress

Y – Parameter used to characterize crack length and component geometry

Y_0 – Initial yield stress

Y_{Sat} – Isotropic saturation stress

ΔK –Stress intensity factor range

ΔK_{th} – Fatigue crack growth threshold

ΔK_{eff} – Effective stress intensity factor

$\Delta \varepsilon^p$ – Plastic strain range in a hole situation

$\Delta \varepsilon_0^p$ – Plastic strain range in a situation without hole

υ – Poisson's ratio

σ – Nominal stress

$\bar{\sigma}$ – Equivalent stress

$\boldsymbol{\sigma}'$ – Deviatoric Cauchy stress tensor

$\sigma^{Fit}(\boldsymbol{A})$ – Fitted true stress

$\sigma^{Exp}(\boldsymbol{A})$ – Experimental true stress

σ_Y – Stress along the y-axis

$\bar{\varepsilon}^p$ – Equivalent plastic strain

ε_0 – Initial plastic strain

$\dot{\bar{\varepsilon}}^p$ – Equivalent plastic strain variation

ε_P – Plastic strain

Σ – Effective Cauchy stress tensor

Acronyms/Abbreviations

AA – Aluminium Alloy

CCP – Centre-Cracked Plate

CCT – Centre-Cracked Tension

CT – Compact Tension

CTOD – Crack Tip Opening Displacement

DD3IMP – Deep Drawing 3D IMPlicit finite element solver

FCGR – Fatigue Crack Growth Rate

GTN – Gurson-Tvergaard-Needleman

HAZ – Heat Affected Zone

LEFM – Linear Elastic Fracture Mechanics

MT – Middle Tension

OICC – Oxidation Induced Crack Closure

PICC – Plasticity Induced Crack Closure

RICC – Roughness Induced Crack Closure

SDH – Stop Drilled Hole

SENT – Single Edge Notched Tension

VH – Vickers Hardness

1. INTRODUCTION

1.1. Motivation

The industry needs to take the most out of their machinery, which means better performance and quality at low cost. This creates challenges for engineers. In fact, as better equipment needs to be designed for such requirements, some of them arise with colossal proportions, where everything needs to be connected and synchronized.

Fatigue phenomenon is one of the major issues with mechanical components, since most of them operate under cyclic loadings, which may originate the growth of pre-existing cracks and the subsequent unstable fracture. This phenomenon is defined as the progressive weakening of a material and may lead to a complete fracture. If not detected in time, which is sometimes challenging, due to the complexity and proportions of certain equipment, it can cause overwhelming losses, requiring the replacement or reparation of the component. Even today, fatigue is an important field of study and discussion since advances in the matter are being achieved little by little. However, it is very important to acknowledge what has already been studied, in order to have a base of understanding. Normally, fatigue design is based either on a required lifetime, for a component, or in the so-called damage tolerance approach. The last one requiring the assessment of fatigue crack growth rates, obtained either numerically or experimentally. Both these approaches have their advantages and disadvantages, which must be considered when the precision of the results, or time availability, are key factors. Understanding the phenomena behind FCG is crucial to improve the fatigue performance of materials and components. In this way, the numerical approach is the one that provides faster results with less costs involved, since many scenarios can be simulated without the need for machinery or the making, and replacing, of physical specimens. However, numerical simulations need input information that can only be obtained via experimental trials. Moreover, numerical results always need confrontation with experimentally obtained data, in order to validate them, which means both approaches need to coexist in order to achieve accurate and reliable results. In this work, a numerical approach based on cumulative plastic strain at the crack tip has been used to predict fatigue

crack growth rate. Crack closure was found to be the main mechanism behind the effects of stress ratio, overloads, and load blocks. However, the relevance of crack closure to explain the effect of geometrical parameters has not been studied yet.

1.2. Objectives

The main objective of this thesis is to study the effect of crack flank holes in fatigue crack growth. Different aspects will be evaluated, namely the holes diameter and positioning, relatively to the crack. The employed numerical model is based on the cumulative plastic strain at the crack tip. Numerical simulations consider CT specimens, made from 2024-T351 aluminium alloy, with five different geometries subjected constant amplitude loading. The in-house developed finite element code, DD3IMP, was employed in all the simulations.

1.3. Layout of the thesis

The layout of these thesis is presented as follows:

- Chapter 1 – Introduction: contains the main subject, motivation, and objectives of this thesis.
- Chapter 2 – Literature Review: contains an explanation of the main subject, as well as some concepts of the fatigue field, namely the Linear Elastic Fracture Mechanics, crack closure and the crack tip opening displacement (CTOD). This chapter also presents information about numerical simulation and historical data, regarding the geometry effects in fatigue crack growth.
- Chapter 3 – Material Model: contains information about the plasticity theory and materials employed. The finite element model is described, and the load conditions are presented.
- Chapter 4 – Results: contains the results obtained in this study, regarding the effect of the holes near the crack tip in fatigue crack growth.
- Chapter 5 – Discussion: contains information about the numerical model used for the experimental trials, namely load conditions, mechanical and chemical proprieties.
- Chapter 6 – Conclusions: the main conclusions about this subject are presented.

2. LITERATURE REVIEW

2.1. Fatigue

"Fatigue" is a term that firstly appeared in the 1840's and was introduced to describe the failure of components that were constantly subjected to cyclic loads. This phenomenon is characterized by the localized, progressive, and permanent structural changes, happening on a component while subjected to fluctuating stresses. Somewhere in time, fatigue crack growth or complete fracture may occur, normally, for values under the tensile strength of the material [1]. The fatigue phenomenon is divided in three main stages: initiation, propagation, and final fracture.

- **Initiation**: The first stage is where the nucleation of the crack and its microscopical growth happens. This process usually starts at the surface, in defects, due to the plastic deformation that results from the application of repetitive load cycles. These loads will induce the formation of slip lines, which may form cracks.
- **Propagation**: There are three usual crack propagation modes: ductile or fragile striation, coalescence of microcavities and microcleavage [2]. Under loading, there is an increase on crack growth rate, normally perpendicularly to the load direction.
- **Final fracture**: In this stage, there is a crack growth rate increase, to a point it becomes unstable, originating sudden fracture since the material can no longer support the applied loads.

Fatigue is the cause of 80 to 90% of failures in engineering components. Since crack growth increases, cumulatively, with the number of load cycles applied, the prediction of fatigue life is extremely important [3]. Indeed, dynamic loads are present in most of the machinery components, like transportation vehicles, structures, shafts, wind related machinery, etc. Therefore, the number of components subjected to fatigue is overwhelming, urging the need to understand this phenomenon.

2.2. Linear Elastic Fracture Mechanics (LEFM)

Usually, design methods are based on an admissible stress, which is defined with a high safety factor. In these methods, the components are normally projected for an infinite lifespan. When it comes to fatigue, traditionally, the crack initiation is not considered for design, due to the application of a dynamic safety factor, which makes fatigue fracture practically impossible. In fact, this methodology leads to components with excessively high proprieties. The Linear Elastic Fracture Mechanics (LEFM) became a main actor in fatigue design as it allows for dimensioning considering a certain lifespan. Therefore, it concedes a good commitment between stresses, defect dimensions and service life.

Fatigue crack growth rates, FCGR, are usually presented through the well-known *da/dN*–ΔK diagrams, such as the one presented in Figure 2.1. These curves show the evolution of the crack growth rate with the range of the stress intensity factor, Δ*K*, given by the difference between the maximum and minimum values of *K* in the load cycle. The stress intensity factor can be calculate using the following expression:

$$K = Y\sigma\sqrt{\pi a}, \tag{2.1}$$

where σ is the nominal stress, *a* is the crack length and *Y* is a parameter used to characterize crack length and component geometry. The intensity factor range is given by Equation 2.2, as such:

$$\Delta K = K_{\max} - K_{\min}, \tag{2.2}$$

where K_{max} is the maximum value and K_{min} is the minimum value of the stress intensity factor in each cycle.

As seen in the Figure 2.1, the graph is divided in three regimes [4]:

- **Regime I:** In this section the crack growth rate depends highly on the stress intensity factor and there's a certain value of Δ*K* below which there's no crack propagation, ΔK_{th}. This is called the crack growth threshold and it can be determined experimentally using several techniques.
- **Regime II:** This section is characterized by a stable crack propagation, which is explained by the linear relationship between crack growth rate and stress intensity factor (in log-log scales). This region is mathematically described by Equation 2.3, representing the Paris-Erdogan Law [5], where *C* and *m* are

material constants, which depend on the material, stress ratio, and environmental conditions.

$$\frac{da}{dN} = C(\Delta K)^m \tag{2.3}$$

- **Region III:** This segment of the graph is characterized by the sudden increase of *da/dN* with ΔK until final fracture, which occurs when K_{max} reaches the material fracture toughness, K_{IC}.

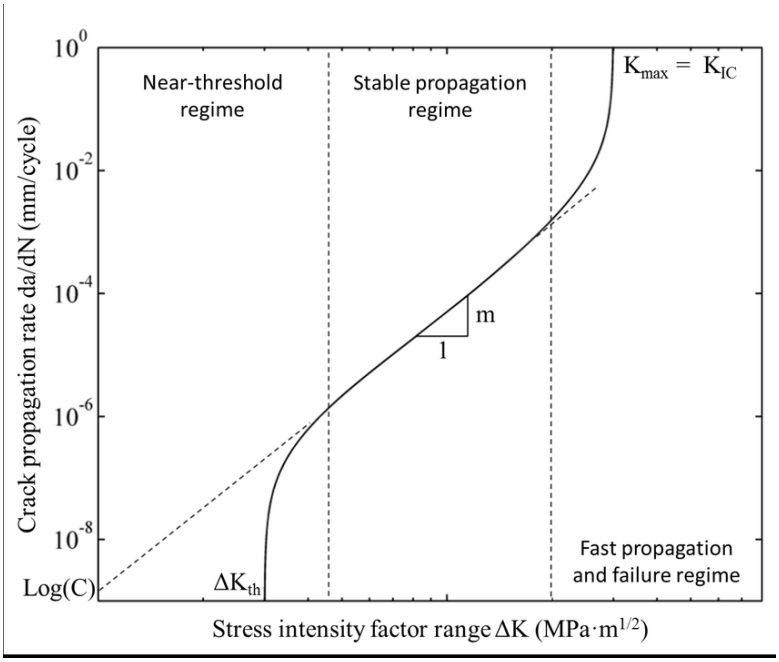

Figure 2.1. da/dN–ΔK graph, in logarithmic scale. Adapted from [6].

2.2.1. Parameters that influence fatigue crack growth rate

There are several parameters influencing fatigue crack growth rates, such as the material properties, the components thickness, the environment conditions and the loading spectrum, among others [4]. Figure 2.2 presents a *da/dN*-ΔK with a stress ratio, $R=0$, and constant stress range. Let us take a closer look to the environment effect, by comparing two different environment conditions. When combining corrosive environments with load frequencies, it is not hard to understand that the lower the frequency, the longer the environment exposure, which allows for a higher degradation rate. The curves will both converge to the material's fracture toughness [7].

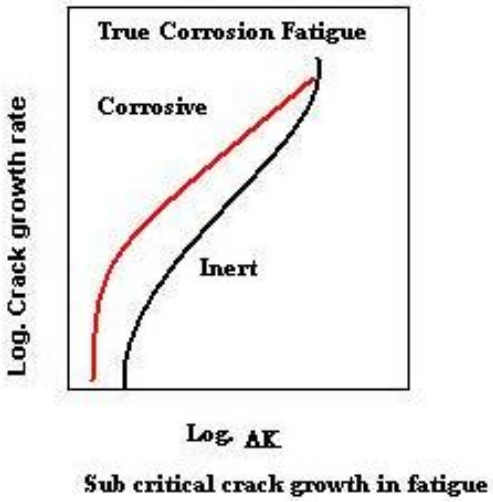

Figure 2.2. Corrosion effect on fatigue crack growth rate. Adapted from [7].

Another factor that changes the *da/dN*–Δ*K* diagrams is the mean stress or stress ratio. When these parameters increase there is an uphill movement of the graph, as shown in Figure 2.3. The increase of *R* will lead to a decrease of the fatigue threshold, ΔK_{th} (if crack growth is verified). It is also noticeable that, for the same value of Δ*K*, the higher the *R* the higher the crack growth rate [4].

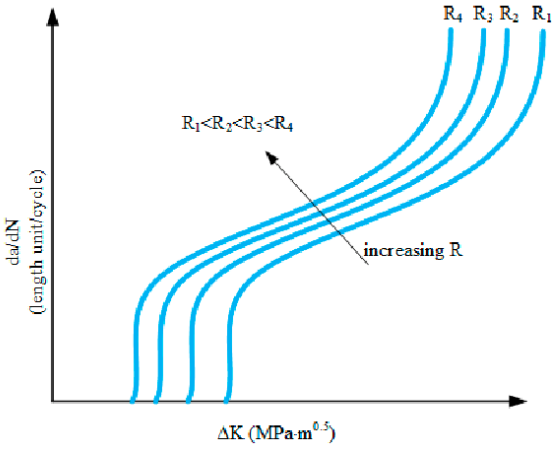

Figure 2.3. Stress ratio effect on fatigue crack growth rate. Adapted from [8].

2.2.2. Issues regarding the application of the LEFM

Fatigue crack growth mechanisms at the crack tip are normally non-linear and irreversible. With this in mind, and knowing that, accordingly to LEFM, FCG at the crack tip

is controlled by the ΔK parameter, there are certain issues that need to be addressed, namely [9]:

- Inability to predict the influence of stress ratio and load history on *da/dN*-ΔK graphs.
- In cracks of small dimensions, there is an odd behaviour.
- Existing dimensional problems with the *da/dN*- ΔK expression:
    - $(\Delta K)^{\mathrm{m}}$ units are $[\mathrm{MPa}\sqrt{\mathrm{m}}]$.
    - *da/dN* units are $\left[\frac{\mathrm{m}}{\mathrm{cycle}}\right]$.

    Which implies that the constant *C* will have as units $\left[\frac{\sqrt{\mathrm{m}}}{\mathrm{MPa}*\mathrm{cycle}}\right]$.
- Validity limited to the Small-Scale Yielding (SSY) condition.

To address this problem, some solutions were proposed to help fulfilling the shortcomings of the LEFM application. These solutions will be discussed in the next section.

2.2.3. Crack closure

One approach, used to study FCG in a more exact way and suppressing the gaps left by LEFM, is the crack closure concept, introduced by Elber [10]. This concept focus on what happens behind the crack tip and is based on the contact between crack flanks, even when the specimen is under tension load. This happens because an elongation is verified in the plastic zone around the crack, which leads to a reduction of the thickness within it and a flow of material to the crack flanks, as shown in Figure 2.5. As the crack propagates, the faces end up contacting with each other, even when the specimen is still in tension [11].

The main mechanisms behind crack closure, presented in Figure 2.4, were discovered by Ritchie *et al* in 1980 [12] and Suresh and Ritchie in 1982 [13], [14] and are named as follows:

- Plasticity induced crack closure (PICC).
- Oxidation induced crack closure (OICC).
- Roughness induced crack closure (RICC).

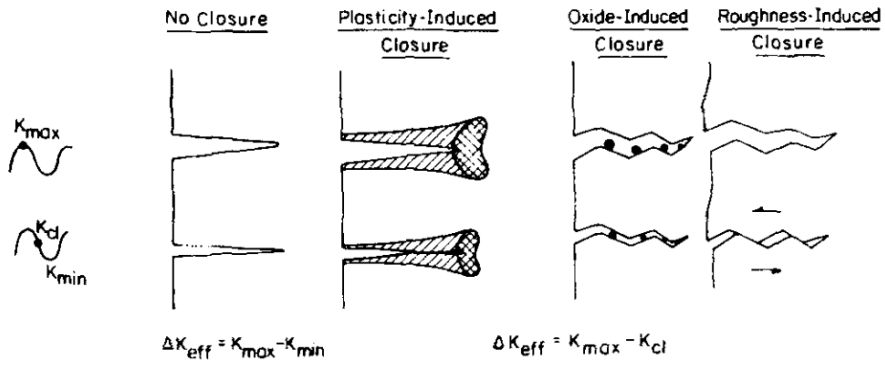

Figure 2.4. Main crack closure mechanisms. Adapted from [14]

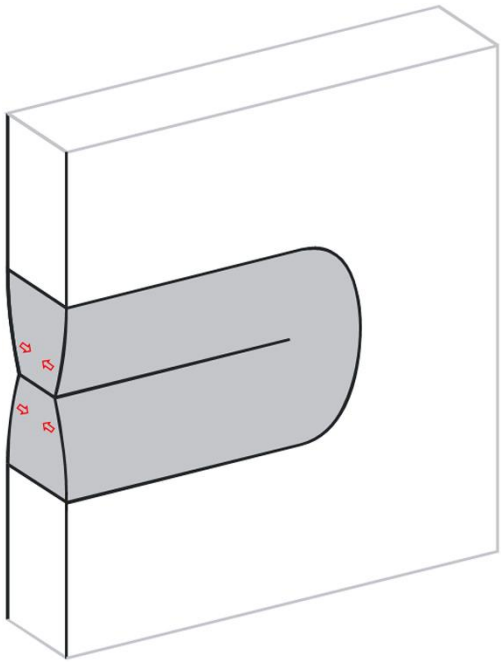

Figure 2.5. Reduction of the thickness in the plastic zone as the specimen in under tension (in plane stress state). Adapted from [11]

Under plane stress state, crack closure can be compared to an extra layer of material, that accumulates behind the crack tip, like a wedge placed between the crack flanks. This phenomenon protects the material, reducing the effective intensity of the stress state and cyclic plastic deformation at the crack tip and, therefore, the crack propagation rate. Since only the portion of the load cycle during which the crack is open contributes for its propagation, an effective value for ΔK (ΔK_{eff}) was proposed. This new parameter being defined by the difference between K_{max} and K_{open} [10], which is the stress intensity factor for the load at which the contact of crack flanks ceases to exist. This means that in the portion of the load cycle below K_{open} the crack remains closed, i.e., below K_{open} there is no crack propagation. Under

plane strain state, there are no deformation along the thickness direction. Thus, plasticity induced crack closure (PICC) shouldn't occur, since the volume of material behind the crack tip has to remain constant.

It is also important to refer that, in the Paris equation, ΔK_{eff} should replace ΔK, as follows:

$$\frac{da}{dN} = C\left(\Delta K_{eff}\right)^{m} \tag{2.4}$$

For low values of ΔK, RICC and OICC are expected to be prevalent, as the crack opening is still small. It is important to note that oxidation induced crack closure strongly depends on the environment conditions and material properties, roughness induced crack closure, on its way, depends on the roughness of the fracture surfaces. In regime II of the *da/dN*-ΔK diagram (Figure 2.1), the plasticity induced crack closure mechanism is supposed to be the most relevant. It consists in the formation of a plastic zone around tip originated by stress concentration.

Additionally, some other mechanisms, present in certain susceptible materials were observed throughout the years:

- Pineau, 1974 [15]: Crack closure induced by graphite.
- Tzou, 1985: Crack closure induced by a viscous fluid.
- Takeshio, 1987 [16]: Crack closure induced by transformation.

Whether numerically or experimentally, there is a vast number or procedures to measure crack closure. Borrego [17] used a global approach, which consisted on retrieving the compliance curve, from a middle-tension specimen (MT), with a small pin-gauge at centre. This method is performed by using the upper 10% of the Force-Displacement data and calculating the least squares correlation coefficient, repeatedly, until a maximum value is reached, which is later defined as F_{open}. This value is then used to calculate the parameter U^*, representing the fraction of the load cycle where the crack remains fully closed, using:

$$U^* = \frac{F_{open} - F_{min}}{F_{max} - F_{min}} \times 100 \tag{2.5}$$

The comprehension of crack closure phenomenon allows, for example, a better understanding of the ΔK_{eff} influence, i.e., if this parameter is (or not) the crack driving force.

$$\Delta K_{eff} = U \times \Delta K \tag{2.6}$$

It is very common to eliminate the effect of the stress ratio on the validation of certain parameters acting as a driving force [18]. Although crack closure helped understand the effect of various variables, such as loading history, its importance in the study of FCG is not consensual among the scientific community.

Some parallel approaches are:

- **T-stress concept**: Used to explain the effect of specimen geometry on crack closure. The T-stresses act parallel to the crack plane. As an example, in 2002, Tong *et al.* [19] tested CT, SENT and CCT specimens, and showed that fatigue crack growth, on a CT specimen, was up to 10 times faster than the measured on the other two geometries. Tong also showed that a tested MT specimen presented constant negative T-stresses, while a CT specimen presented positive T-stresses, that increased as the crack became longer Additionally, their sign and magnitude showed a great influence on the shape of the plastic zone near the crack tip.
- **CJP concept**: Christopher et al. [20], [21] proposed a new mathematical model to characterise the stresses around the crack tip. This model considers plasticity through its protective effects on the applied elastic field. To characterize the plastic field, four parameters were used:
    - Opening mode stress intensity factor, K_F.
    - Shear stress intensity factor, K_S.
    - Retardation stress intensity factor, K_R: characterizes the protective effect on the crack that can come from plasticity at the crack tip and at the wake.
    - T-Stress.

All the previous proposals are based on the ΔK parameter. However, as mentioned before, there are some limitations related to this parameter's linear nature. Therefore, new models were developed, being based on non-linear parameters such as the crack tip plastic strain, crack tip opening displacement (CTOD), dissipated energy and cyclic cumulative plastic strain.

2.3. Numerical Simulation

The experimental approach is not always the fastest and most convenient way to determine FCG related parameters, due to its dependency on so many factors, such as the mechanical properties of the component's material. Therefore, numerical simulation can be extremely helpful.

A numerical method basically consists in converting a physical problem or model to a mathematical form, so it can be solved numerically instead of analytically. This can be useful, for example, when a certain process is not possible to describe analytically. The finite element method for this model must be simplistic to a point where the final results are not compromised, so that precise results are obtained with the least computation effort possible.

A physical model describes a certain component, machine, or system on a smaller scale. The correspondent mathematical model can represent the whole physical component or just a portion of it, if the correspondent boundary conditions reflecting the "missing" part of said component are given. It should be detailed according to the resources available, as this should be a good compromise between computing capacity and data accuracy.

Numerical simulation comes with a lot of benefits, as this approach can help gather information that otherwise would be expensive due to experimental procedures or even be impossible. Here are listed some of them:

- Increased understanding of the correspondent physical model, adding to or by comparison with experimental results.
- Simulation of unfamiliar situations, as it allows the user to change parameters that would be hard to physically impose.
- Very flexible approach, as it is possible to explore different geometries and operating conditions.
- Problem/Failure prevention and tracking, through 3D simulations (for example stress and strain analysis) which can help prevent the failure of a certain component, therefore understanding which areas are affected.

In this work the simulation of FCG is made through a node release strategy, which is based on running through the mesh, increasing a node every time the cumulative plastic strain reaches a critical value [22]. This method shows fast stabilization, and it is independent from the node release load. There are some distinctive methods considering the node releasing instant. In 1986, Fleck [23], had a node release scheme that consisted in releasing a node when

maximum load was achieved, in every load cycle. This scheme was used throughout the years by most of the investigators. McClung *et al.* [24] in 1990, would implement the release of a node at minimum load, every load cycle. Another possible approach used by Wu and Ellyin [25], in 1996, consisted in releasing a node every load cycle, but this time, at maximum and minimum load. Among these, releasing a node at maximum load every two load cycles (Zhao *et al.*[26], 2004) and at minimum load every two load cycles (Alizadeh *et al.*[27] , 2006) were also considered.

2.4. Effect of Geometry

2.4.1. Type of Specimen

As mentioned before, geometry is one of the main parameters affecting fatigue crack growth rates, as verified by Fleck in 1986 [23], who studied two different specimen geometries, namely a centre cracked panel (CCP) and a Bend specimen. In his work, Fleck noted that, in the Bend Specimen, for $K=K_{max}$ the T-stresses were positive, reinforcing the existing plastic zone, which was "similar to that of a tearing crack" [28]. After unloading to K_{min}, the T-stresses became negative and beside the crack flanks there was an elastic zone. Additionally, the crack tip was surrounded by reverse plastic zone. For the CCP specimen, at K_{max}, the T-stresses were negative and there was no secondary plastic zone (active yield zone along the crack flanks, due to tearing of the material). After unloading to K_{min}, the T-stresses became positive, and the secondary plastic zone reappeared.

2.4.2. Thickness

An important parameter that requires our attention is the specimen's thickness, as it can greatly influence its behaviour in service, namely in FCG rates (da/dN-ΔK). The increase of the thickness leads to an increase of the da/dN. Costa and Ferreira [29], 1998, concluded that, for lower values of stress ratio (R=0), the thickness would have a bigger influence on FCG rate (Figure 2.6), whereas this influence would be smaller for higher values of ΔK.

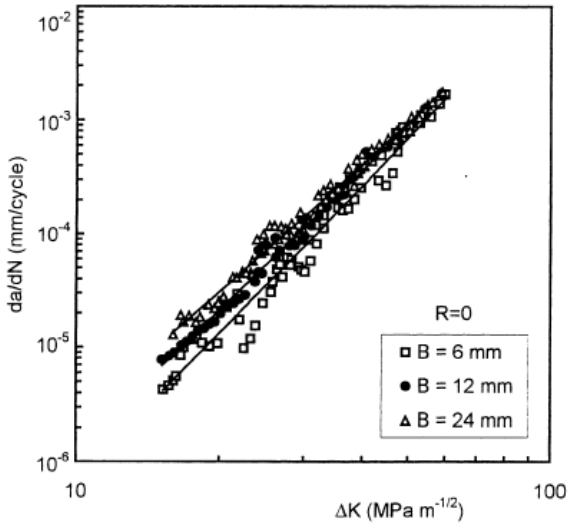

Figure 2.6. Thickness effect on FCG rate. Adapted from [29].

Smaller thicknesses would also influence the crack closure load parameter *U* in a more noticeable way, as can be seen in Figure 2.7. The crack closure increases with the decrease of the thickness. Wang *et al.,1999* [30], studied the influence of this parameter and concluded that the bigger the specimen's thickness, the lower would be the ratio between the opening and the maximum applied stresses. Figure 2.8 shows the thickness effect on crack opening stresses in a centre-cracked tension (CCT) specimen.

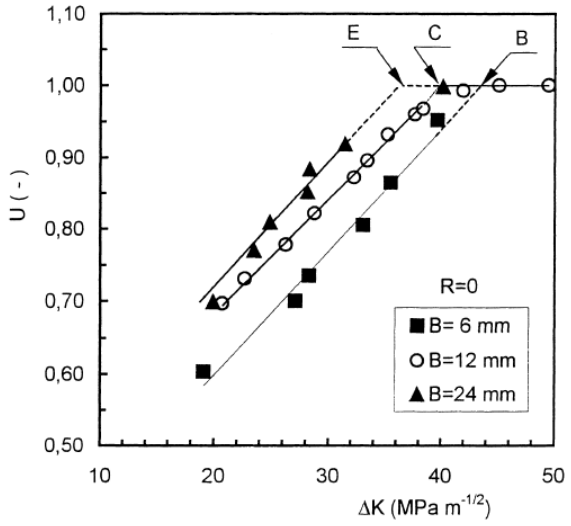

Figure 2.7. Thickness effect on crack closure load parameter. Adapted from [29].

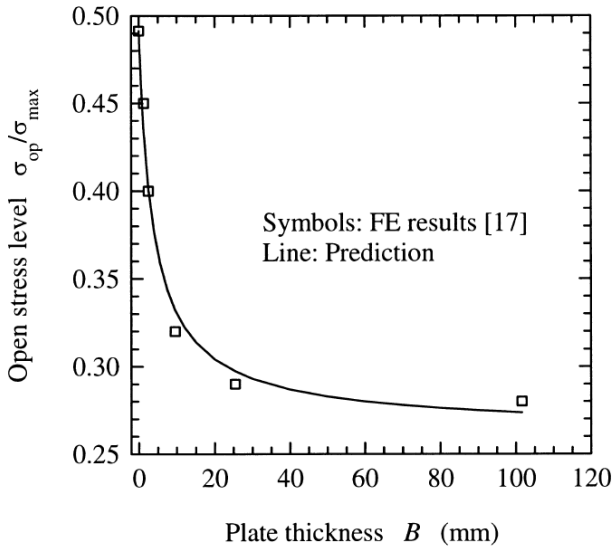

Figure 2.8. Thickness effect on crack opening stress in a CCT specimen. Adapted from [30].

There is no significant thickness effect when *da/dN* is plotted versus CTOD. These results can be seen in Figure 2.9. Both measurements were made for the same values of Δ*K*.

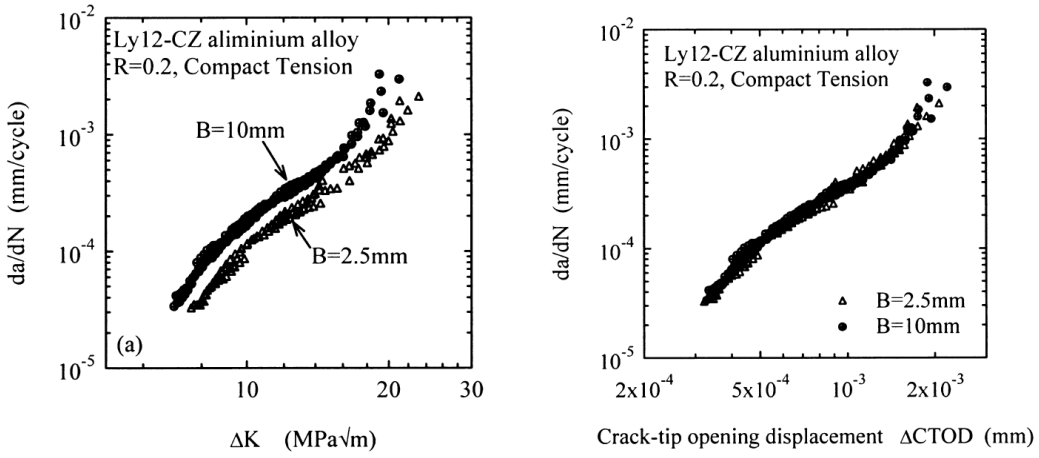

Figure 2.9. Thickness effect on FCG rate and CTOD. Adapted from [30].

2.4.3. Constraints

A constraint, in this case, can be understood as something that decreases FCG rate or prevents deformation to happen when a specimen is under load, such as thickness or holes. Hutař *et al.*, 2004 [31] studied the effects of constraints in the fatigue crack growth rate for different geometries based on a phenomenological approach assuming linear elastic fracture mechanics with two parameters constraint-based. The different levels of constraint near the crack tip were quantified using T-stresses, which depends on the geometry of the component.

They concluded that under small scale yielding conditions, for a high load cycle, the lower the constraint level, the higher the fatigue crack growth rate will be. Two different specimen geometries were used: centre cracked plate tension (CCT) and compact tension (CT). It was verified that the CT specimen would have a higher level of constrain, corresponding to positive T-Stress, whereas the CCT specimen would show lower constraint level, i.e., negative T-Stress (see Figure 2.10).

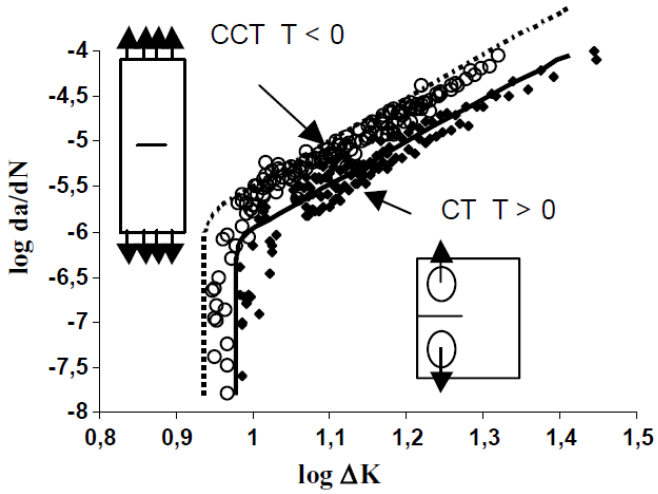

Figure 2.10. Geometry effect on FCG rate analysed through constraint level. Adapted from [31].

2.5. Fatigue crack growth retardation and/or arrest methods

The generation of cracks in components while on service is very common as they are constantly under cyclic loads. Manufacturing itself can produce defects on the components' structure, either by welding, machining, or casting, which might be a starting point for a crack to grow and possibly end up in failure. Hence, the diagnosis and control of such growth is very important. There are many methods [32] that can prevent the growth of a crack and thus extend the fatigue life of a structural component, especially in situations where it cannot be replaced as soon as the crack is identified, such as:

- Crack filling: Infiltrated materials can affect ΔK_{eff}. This was shown, in 1979, by Kitagawa *et al.*[33], who verified that an artificial wedge would significantly reduce crack growth rate and, if certain conditions were verified, the growth process could even cease. Years later, Yanyan *et al.* [34] used industrial glues to infiltrate cracks in steel sheet specimens and although fatigue crack growth arrest

wasn't verified, there was retardation. Also, in 1997, Sharp *et al.* [35], using an aluminium alloy 7050-T73651, (used in military aircraft) ,verified that for 50% infiltration stress level, the specimen's fatigue life would suffer an increase from 30 to 50%, comparing to 0% infiltration stress level. The fatigue life of the specimen of each test is shown in Table 2.1.

Table 2.1. Specimen fatigue lives after adhesive infiltration. Adapted from [35].

	0 %ISL (0 kN) cycles	50 %ISL (2 kN) cycles	80 %ISL (3.6 kN) cycles
No Adhesive	30 023	----------	28 945*
Epoxy 1	32 146	38 681	112 006
Epoxy 2	29 888	44 655	960 273

*Control specimen held under load at 80%ISL, but without adhesive.

- Application of metallic composite patches on the cracked surface [36]: Ayatollahi *et al.* has shown that the use of composite patches (due to its high strength and formability) would substantially reduce the stress intensity factor ΔK_{eff}, therefore reinforcing the existing crack and reducing crack growth rate.
- Welding repair [37]: Zhang *et al.* studied the effect off weld-repairing a high-strength low-alloy steel on its fatigue life, by measuring Vickers Hardness (VH) for various situations. It was observed that the VH values in the region that contained the buffer layer (intermediate material deposit between the base material and the weld metal) and the heat affected zone (HAZ) were reduced and the alloy's fatigue resistance was substantially improved.
- Compressive stress application: There are many methods to apply compressive stresses, such as overloading [38], indentation [39], laser-generated shocks [40], [41], shot peening [42], spot heating [43] and, the most important method for this thesis, drilling holes near the crack tip [44]–[48]. All of the methods mentioned above aim to reduce the risk of failure initiating from tensile stresses.

2.6. Influence of holes on fatigue life

Drilling holes in the vicinity of the crack tip is a very popular way to increase the fatigue life of a material specimen as it turns the crack tip into a notch, reducing the stress intensity factor [49]. Throughout the years, many approaches were tested, varying the number, position, and size of the holes, in order to achieve a longer fatigue life or eventually stop the crack from propagating and, therefore, preventing catastrophic failure. A very common technique used is called the stop drill hole method (SDH) and it consists of drilling a single hole next to the crack tip, stopping the crack propagation, as can be seen in Figure 2.11.

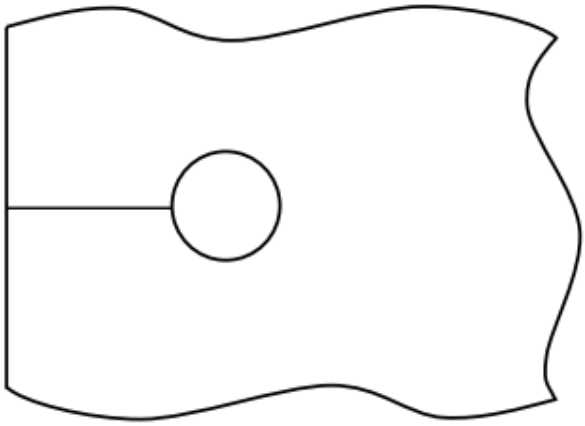

Figure 2.11. Stop Hole Technique. Adapted from [49].

Shang *et al.* [44] tested this method by drilling stop-holes with 2 mm, 2.5 mm and 3 mm near the crack tip to ensure its removal and observed that, the fatigue life would improve with the increase of the hole diameter, as shown in Figure 2.12.

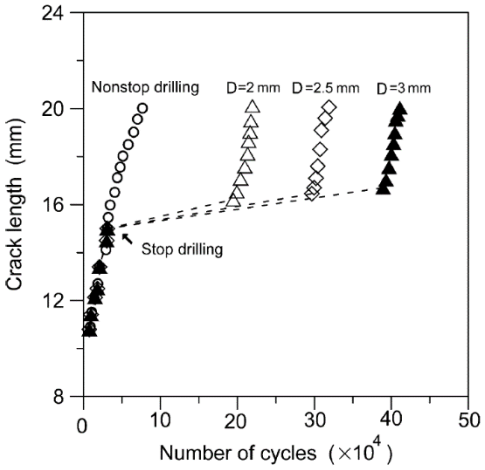

Figure 2.12. Effect of stop-hole diameter fatigue life and crack initiation. Adapted from [44].

In 2015, Ayatollahi *et al.* tested a different approach, consisting of drilling two holes in the crack tip in a way that it will reduce the stress concentration at the edge of stop-holes while also reducing the singularity at the crack tip. One aspect to have in mind is the material loss from drilling. This method is represented in Figure 2.13. With this analysis it was concluded that the concentration zones would be divided by the two holes instead of being concentrated in just one, therefore being significantly lower when using the double-stop hole technique when comparing with the single stop-drill hole method, which resulted in longer crack initiation times. This means that fatigue crack growth rates became smaller, thus increasing the component's fatigue life. This method also allowed to understand that drilling two smaller holes instead of a bigger single hole would account for less material loss.

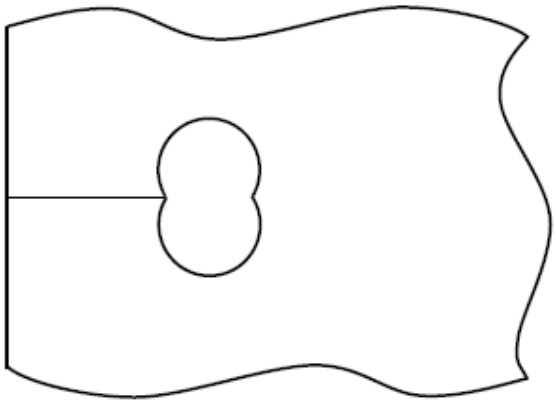

Figure 2.13. Double-Stop Drill Hole Technique. Adapted from [49].

Another technique, studied by Makabe *et al.* [46] also employed the use of drilled holes to arrest or retard crack growth, but in some cases, pins would be inserted into said holes in order to change growth direction and prevent coalescence of crack growing from the specimen's edges. This can be seen in Figure 2.14. It was also found that the insertion of pins would induce residual compression stresses which contributed to slower crack growth rates. This was proven more effective than drilling holes to reduce stress concentration around the crack tip. Therefore, combining the two procedures would be the best solution to retard fatigue crack growth rates while preventing cracks from merging together.

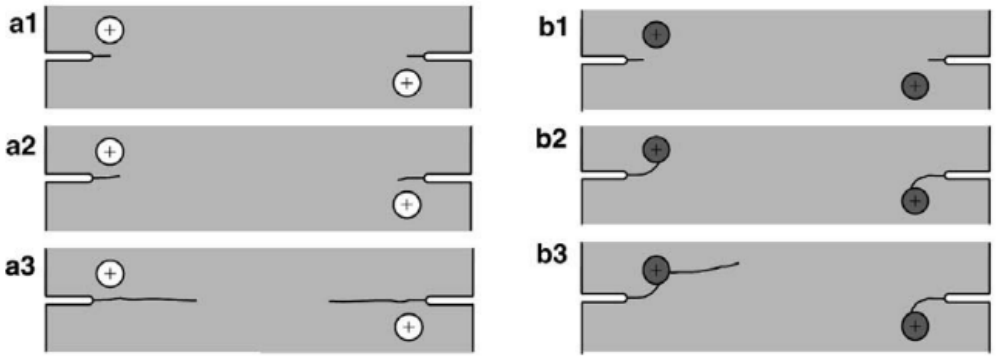

Figure 2.14. Effect of the pins (on the right) in crack growth deviation, when comparing with their absence. Adapted from [46].

Although more than once was proven that drilling holes near the crack tip is an effective way of arresting or retarding crack growth, according to Chen *et al.*[50], the effects of location and diameter of the holes when studying low cycle fatigue, namely on the ratchet limit and crack tip plastic strain range, have not been studied thoroughly. It is important to note, for easier comprehension, that the ratchet limit refers to the maximum plastic strain that can be taken by the component while under cyclic loads and that it is a very important issue to be addressed, as it can cause intolerable deformations. A CT specimen was subjected to cyclic tensile loading and bending moments, as it is shown in Figure 2.15, which contains symmetric holes drilled. Results show that for the same vertical position and diameter, having holes behind the crack tip will not have an effect on the ratchet limit. On the other hand, holes placed ahead the crack tip yields a ratchet limit decrease, making it easier for ratchetting to occur, as shown on Figure 2.16.

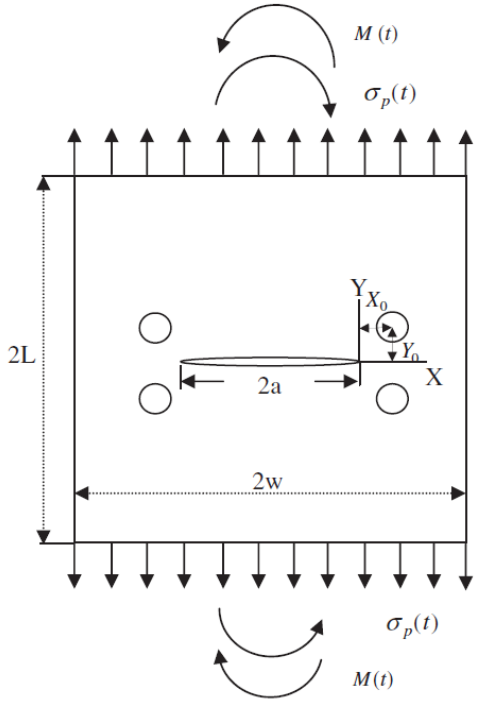

Figure 2.15. Centre cracked plate subjected to bending moments and cyclic tensile loading used to study the influence of drilled holes on the ratchet limit and crack tip plastic strain range. Adapted from [50].

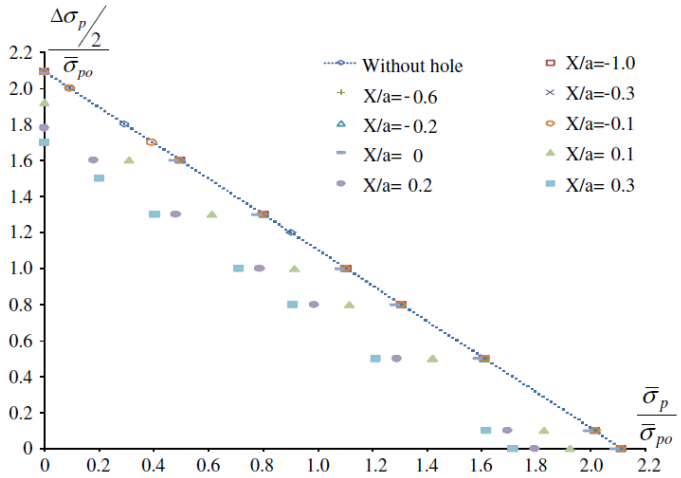

Figure 2.16. Hole horizontal location effect on ratcheting, for the same vertical position. Adapted from [50].

It was also observed that the diameter of the hole will have a bigger influence on the plastic strain range when it is vertically positioned closer to the crack, diminishing the influence as the hole's vertical location increases. We can also see that, for a certain position, the diameter has no influence whatsoever, as shown in Figure 2.17.

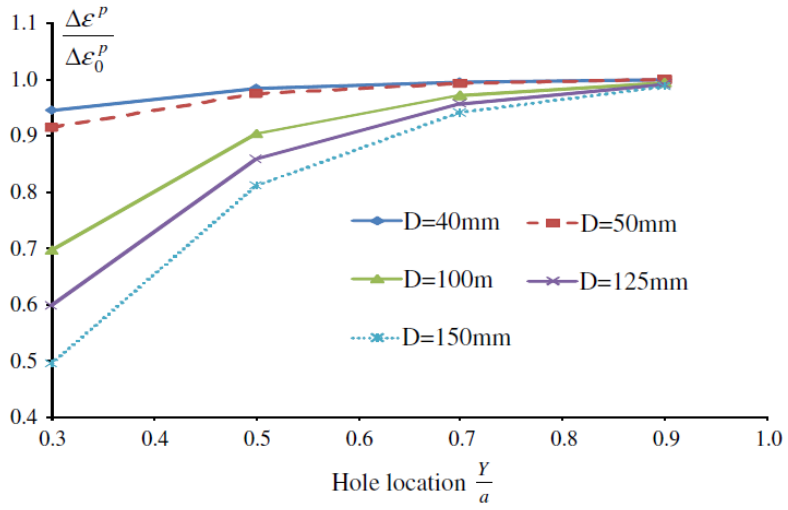

Figure 2.17. Hole vertical location and size effect on plastic strain range. Adapted from [50].

This way, Chen *et al.*[50] concluded that a bigger hole placed vertically closed to the crack would contribute to a 50% reduction of the plastic strain range in a hole situation ($\Delta\varepsilon^p$), when comparing to a situation without hole ($\Delta\varepsilon_0^p$).

3. MATERIAL MODEL

In order to accurately perform the numerical simulation of the FCG, the elastic-plastic behaviour of the material must be addressed. There are several models used to study this behaviour, based on three criteria: the yield criterion, the plastic flow rule, and the hardening law. The yield criteria are employed to describe the elastic behaviour limit in a multidimensional stress field. The plastic flow rule is used to establish a relationship between the stress state and the plastic strain increment. Finally, the hardening law, describes the elastic limit behaviour evolution as the plastic deformation process occurs.

3.1. Yield Criteria

The yield criterion can be divided in two main groups: isotropic and anisotropic. In the isotropic case, the material proprieties remain the same, regardless of the loading direction. It is common to address this matter using two distinct criteria: Tresca [51] and von Mises [52]. Figure 3.1 shows the representation of the stress space for both criteria, in 2D and 3D.

In the present work, the von Mises yield criterion will be adopted, which surface is given, in the principal stress space by:

$$(\sigma_1 - \sigma_2)^2 + (\sigma_1 - \sigma_3)^2 + (\sigma_2 - \sigma_3)^2 = 2{\sigma_0}^2 \tag{3.1}$$

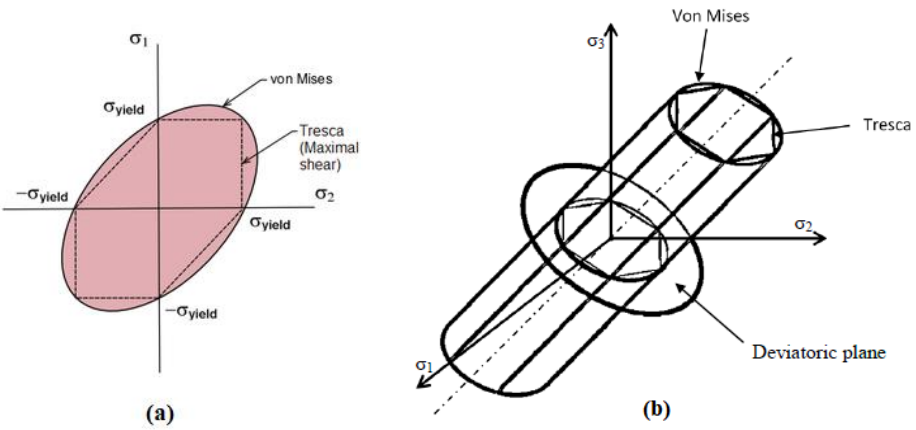

Figure 3.1. Yield surface representation in 2D (on the left) and 3D (on the right) for Tresca's and Von Mises' criteria.

3.2. Hardening Law

Hardening (or softening) is a phenomenon, characteristic from metals and their alloys, that consists in the variation of the flow stress with the evolution of plastic strain. In this work, the two types of laws that describe the yield surface behaviour, when the yield stress is exceeded, are isotropic and kinematic hardening.

3.2.1. Isotropic hardening

In isotropic hardening the yield surface will expand homothetically, keeping its original shape, as shown in Figure 3.2. It is assumed that, independently of how a certain stress state is reached, the final surface is the same [53].

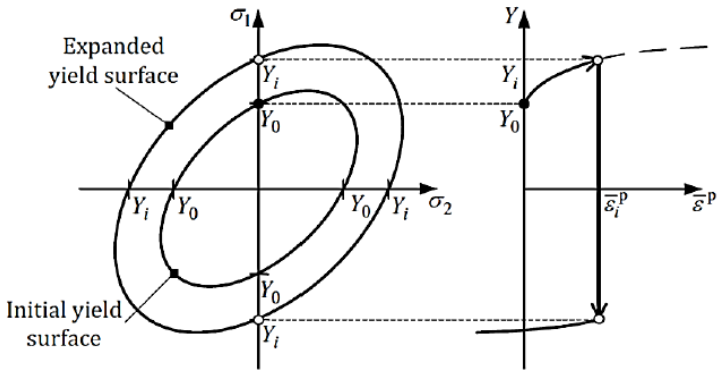

Figure 3.2. Yield surface evolution in isotropic hardening (on the left). Stress-strain curve (on the right). Adapted from [54].

Some important isotropic yield models were proposed by Voce [55] and Swift [56]. The equations for these laws are listed in the Table 3.1.

Table 3.1. Isotropic hardening models proposed.

Model	Equation
Voce	$Y = Y_0 + (Y_{sat} - Y_0) \times \left[1 - exp\left(-C_Y \times (\bar{\varepsilon}^p)\right)\right]$
Swift	$Y = K \times (\varepsilon_0 + \bar{\varepsilon}^p)^n$
Y_0, K, Y_{sat}, C_Y, ε_0 parameters depend on the material	

3.2.2. Kinematic hardening

While isotropic hardening changes the yield surface size, keeping its form, in the case of kinematic hardening the shape and size of the yield surface remains the same, but its centre

suffers translations, as displayed on Figure 3.3. Due to this fact, kinematic hardening laws are recommended for describing plastic deformations under strain path changes. Specially, when the material shows the Bauschinger effect [54], which consists in a drop in yield strength in the opposite direction of the applied force. Table 3.2 presents the equation of kinematic hardening given by Lemaitre-Chaboche.

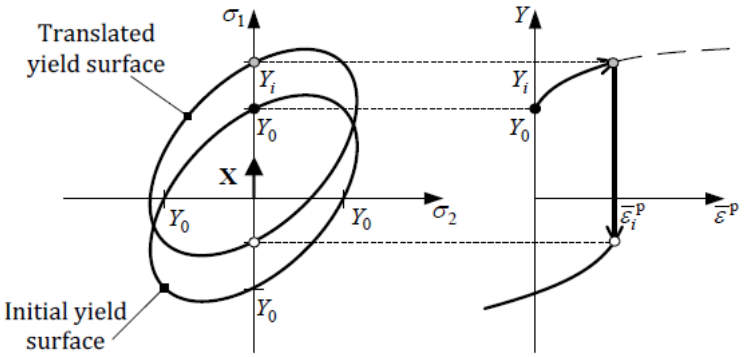

Figure 3.3. Yield surface evolution in kinematic hardening (on the left). Stress-strain curve (on the right). Adapted from [54].

Table 3.2. Kinematic hardening model proposed by Lemaitre-Chaboche [57].

Model	Equation
Lemaitre-Chaboche	$\dot{\boldsymbol{X}} = C_{\mathrm{X}}\left[\frac{X_{\mathrm{sat}}}{\bar{\sigma}}(\boldsymbol{\sigma}' - \boldsymbol{X})\right]\dot{\bar{\varepsilon}}^{\mathrm{p}}\ with\ \dot{\boldsymbol{X}}(0) = 0,$
C_X, X_{Sat} : parameters depend on the material X represents the back stress tensor and $\sigma'$is the deviatoric components of the Cauchy stress tensor, $\boldsymbol{\Sigma} = \boldsymbol{\sigma}' - \boldsymbol{X}$	

3.3. Materials

The material used in this study is the 2024-T351 aluminium alloy, which chemical composition is presented in Table 3.3.

Table 3.3. Chemical composition for 2024-T351 aluminium alloy, in weight (%)

Al	Si	Fe	Cu	Mn	Mg	Cr	Zn	Ti
Bal.	0.5	0.5	3.8-4.9	0.3-0.9	1.2-1.8	0.1	0.25	0.15

The calibration of elastic-plastic parameters is crucial to describe a material through a constitutive model, this way it is a fundamental step to achieve an accurate numerical solution. In order to calibrate these parameters, an elastic-plastic model is considered. The elastic behaviour is assumed isotropic, being defined by the generalized Hooke's Law. The values assumed for the Young Modulus and Poisson's coefficient are presented in Table 3.4 [58]. The yielding behaviour is given by the von Mises criterion, where its evolution is described by the Swift isotropic hardening law combined with the non-linear kinematic hardening law of Lemaitre-Chaboche. The von Mises surface, used to describe the plastic yielding, can be written using:

$$(\Sigma_{22}-\Sigma_{33})^2+(\Sigma_{33}-\Sigma_{11})^2+(\Sigma_{11}-\Sigma_{22})^2+6\left({\Sigma_{23}}^2+{\Sigma_{13}}^2+{\Sigma_{12}}^2\right)=2{Y_0}^2 \quad (3.2)$$

where $\Sigma_{11}, \Sigma_{22}, \Sigma_{33}, \Sigma_{12}, \Sigma_{13}, \Sigma_{23}$ are the components of the effective Cauchy stress tensor and Y_0 is the initial yield stress. Plastic deformation is firstly achieved when the von Mises equivalent stress, $\bar{\sigma}$, matches the initial yield stress. The optimization procedure is performed so that the material parameters that best describe the alloy's cyclic plastic behaviour are obtained by minimizing the least-squares objective function $F(\mathbf{A})$, expressed by:

$$F(\mathbf{A})=\sum_{i=1}^{N}\left(\frac{\sigma^{\mathrm{Fit}}(\mathbf{A})-\sigma^{\mathrm{Exp}}}{\sigma^{\mathrm{Exp}}}\right)_i^2 \quad (3.3)$$

where $\sigma^{\mathrm{Fit}}(\mathbf{A})$ and σ^{Exp} represent the fitted and the experimentally measured values for the true stress on the data point i, respectively. N is the number of experimental data points and A is composed by C_X, X_{Sat}, k and n (see Table 3.4) which are the material parameters to be identified since the Swift law was employed to describe this aluminium alloy. These parameters are obtained through the low cycle fatigue tests. The minimization of F(A) is achieved using an optimization algorithm (Generalized Reduced Gradient, GRG2, [59]) available in the Microsoft Excel SOLVER tool. The mechanical properties describing the elastic-plastic behaviour are presented in Table 3.4 [60].

Table 3.4. Mechanical properties for the 2024-T351 aluminium alloy. Adapted from [60].

Young Modulus [GPa]	**Poisson's Coefficient**	**Swift's Law**			**Voce Hardening Law**	
		Y_0 [MPa]	K [N]	n	Y_{Sat} [MPa]	C_Y [mm]
72.26	0.29	288.96	389	0.056	111.84	138.80

3.4. Specimens

In order to numerically study the holes effect near the crack tip five geometries were created, based on a CT (compact tension) specimen. Each geometry is described in Table 3.5. In Figure 3.4 there is a representation of the CT specimen, where *D* and *V* are drilled hole's diameter and vertical position, regarding the specimen's symmetry axis, respectively.

Table 3.5. CT specimen dimensions and location of the drilled holes.

Characteristic Dimension [mm]	Initial crack length, a_0 [mm]	D [mm]	V [mm]
36	15	Without hole	
		0.5	1
		1	1
		1.5	1
		1.5	1.5

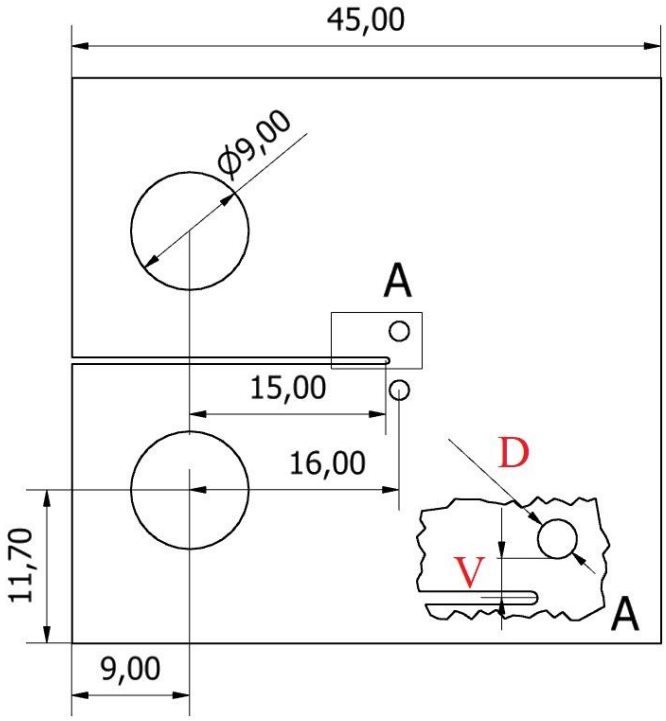

Figure 3.4. CT specimen geometry with hole near the crack tip, which position is defined by its diameter (*D*) and vertical position in relation to symmetry axis (*V*).

3.5. Finite element model

This finite element analysis was performed with the, in-house developed, finite element code DD3IMP, which was originally developed to simulate sheet metal forming processes [61]. Different input files are required, regarding different numerical and physical parameters, which need proper attention:

- DD3_bcon.dat ➔ imposes the boundary conditions on the model
- DD3_contact.dat ➔ in this case imposes contact (or no contact) between crack flanks when unloading. (Note that "no contact" can lead to unrealistic situations such as the crack flanks penetration, but it helps to discard the contact influence on the final results.)
- DD3_input.dat ➔ contains numerical parameters such as and the type of output data, tolerances, residues, and maximum number of iterations.
- DD3_mater.dat ➔contains material data such as the parameters for the constitutive laws.
- DD3_mesh.msh ➔ this file characterizes the finite element mesh.
- DD3_phase.dat ➔ contains the load parameters and respective conditions.

- DD3_tool1.msh➔ in this case contains the geometry of a plane surface, in y=0, that will simulate the contact between crack flanks.
- DD3oCYCLIC.dat ➔ this file describes the propagation criterion, as well as the critical plastic strain value.

The files listed above are needed to start the simulation. When the simulation is completed, there are some files to analyse important parameters like crack growth rate, CTOD, plastic strain, etc.

- R_LINE1_CTOD.DD3 ➔ this file contains the crack tip opening displacement values in the node immediately behind the crack tip.
- R_NODESreleased.DD3 ➔ shows every propagation made throughout the simulation and the respective information, such as the corresponding cycle. This file will be used to determine fatigue crack growth rate.
- R_TIP_DD3 ➔ contains values for the stress and strain states, at the crack tip node(s), in every increment of the simulation.
- ToolBCIDy.res ➔ contains the applied force evolution, through the load cycles, in every increment of the simulation.

3.5.1. Finite element mesh

Due to the symmetry in loading and geometry, it is possible to consider only 1/4 of the specimen, using adequate boundary conditions. The mesh was built in a way that, based on the available time, the results would be as accurate as possible.

Therefore, it has the following characteristics:

- Element size in the zone where the crack will propagate: 0.008 mm (8 μm)
- Average elements dimension in the crack vicinity: 0.2 mm
- Thickness: 0.1 mm

Figure 3.5 represents the finite element mesh for one of the analysed geometries. Note that, every mesh has the same configuration, only changing the number of subdivisions on the small hole in order to achieve a smooth transition between element sizes in the different zones. The finite elements are linear hexahedral and in total, the mesh is built with 14642 elements and 29868 nodes.

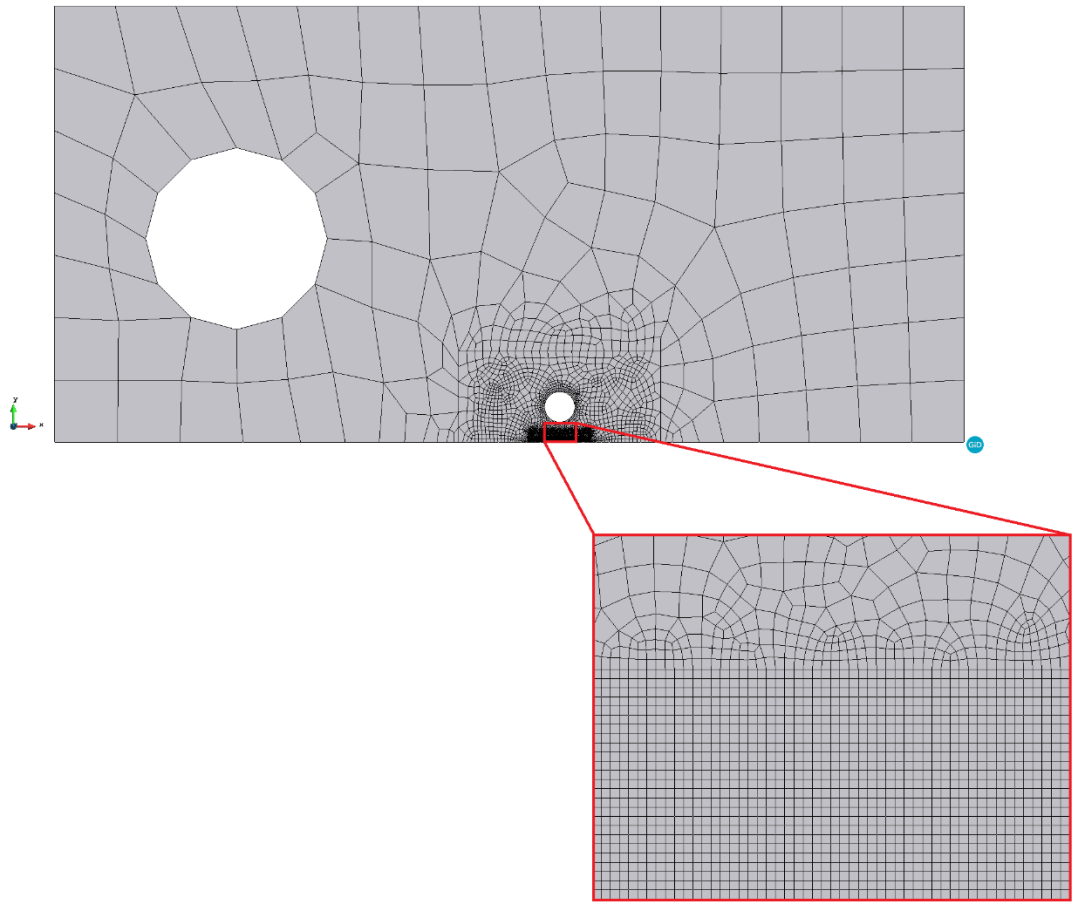

Figure 3.5. Finite element mesh of one of the geometries (D=1.5 mm; V=1.0 mm)

3.5.2. Load

This study considers a constant amplitude load, ranging from $F_{min} = 3.5\ N$ to $F_{max} = 35\ N$, and therefore, R=0.1. Figure 3.6 represents a typical curve, characterizing this type of loading. The load values appear to be small, however e only 0.1 mm of thickness is considered. All specimen geometries, listed in Table 3.5, were loaded assuming both plane strain and plane stress states.

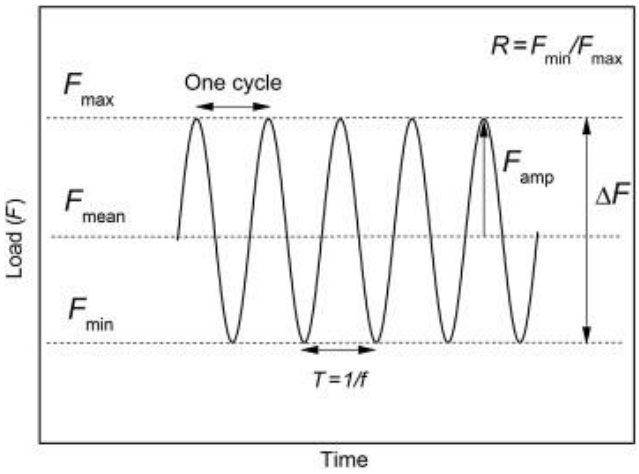

Figure 3.6. Typical Loading-Time curve.

3.5.3. Crack propagation

Crack propagation is done by node release, where each crack increment corresponds to a length of 8μm. Propagation happens when the cumulative plastic strain at the crack tip, ε_p, reaches a critical value. The equivalent plastic strain is measured at the two Gauss points immediately behind and ahead the crack tip, being the plastic strain value, at the crack tip, the average between these two values. The critical plastic strain for a node release is supposed to be a material property.

Figure 3.7 shows an example of the evolution of plastic strain at the crack tip throughout the load cycles. Each drop in the plastic strain correspond to a crack propagation.

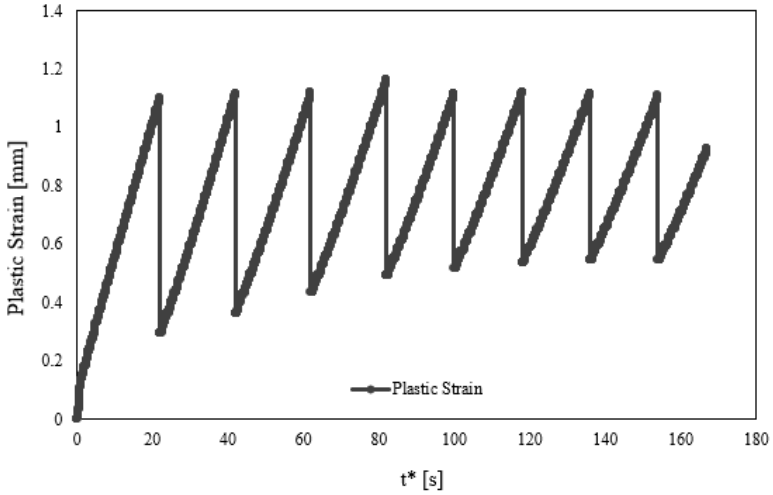

Figure 3.7. Example of plastic strain evolution with time (normalized, t*), for a 17 mm crack length, for a specimen with a 1.5 mm diameter hole, a vertical position of 1 mm, in plane stress state.

In order to determine the critical value of plastic strain, a calibration procedure must be performed, by comparing an experimental value of *da/dN*, for a specific crack length and stress ratio, with the *da/dN*, predicted numerically, for different values of critical plastic strain [22]. Thus, if two points corresponding to different plastic strain values are chosen, one below and one above the *da/dN*-$\Delta\varepsilon_{pc}$ curve, an interpolation can be done to find out the critical plastic strain value, that corresponds to the intersection between the line containing the two chosen points and the *da/dN*-$\Delta\varepsilon_{pc}$ curve. The critical value for $\Delta\varepsilon_{pc}$ used to perform this study was 110%.

4. RESULTS

This chapter presents the numerical results obtained with the numerical model described above. The simulations were performed for plane stress state and plane strain state. The effect of the hole's diameters and vertical position on the FCG was analysed.

4.1. Crack growth rate

The fatigue crack growth rate is here evaluated under different situations. The effect of both the vertical position and the hole diameter on the predicted fatigue crack growth rate is assessed, comparing with the situation without holes. For all situations analysed, the small holes are located near the crack flanks (see Figure 3.4), specifically at a position equivalent to a crack length of 16 mm.

4.1.1. Effect of the hole presence

Figure 4.1 shows the effect of the existence of a hole, on fatigue crack growth rate, considering the same vertical position and diameter, for plane stress and plane strain states. The results show that the hole induces an increase on the FCG rates, right from the start, in both cases. Additionally, both curves intersect when the crack is close to the centre of the hole, for a crack length, a=16 mm, followed by a decrease relatively to the specimen without hole. As the hole's influence fades, there is a rise on FCG rate until this value equals those for the situation with no hole. Under plane strain and plane stress states, the behaviour is similar, with the initial FCG values being slightly higher in the second.

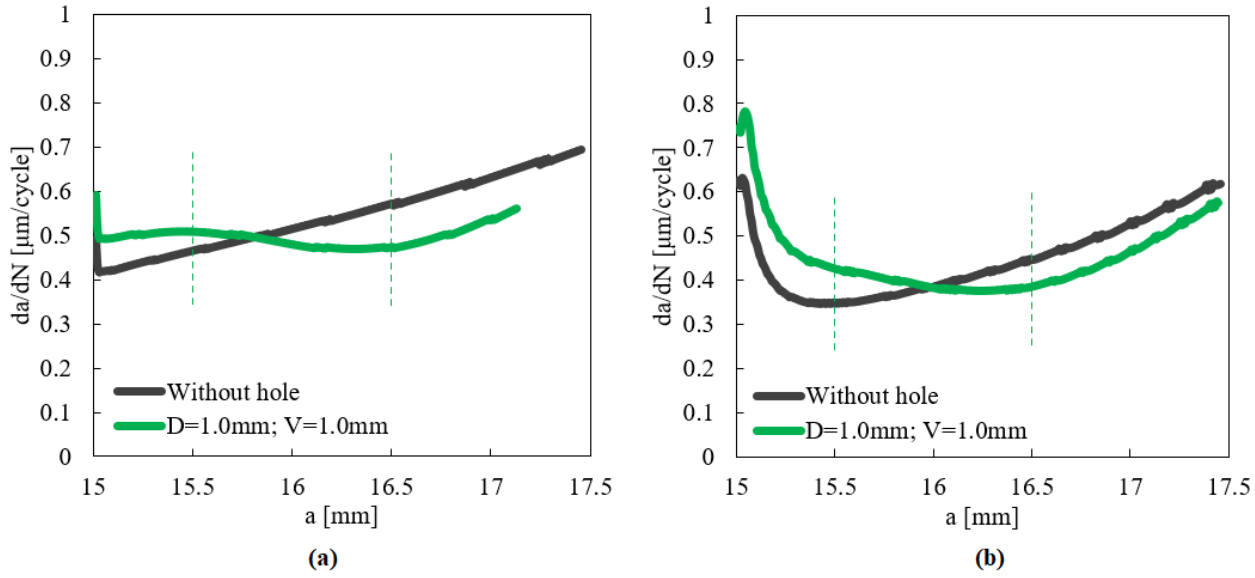

Figure 4.1. Effect of the hole presence on FCG rate for the same vertical position: (a) plane strain state; (b) plane stress state.

4.1.2. Effect of the hole diameter

Error! Reference source not found. presents the effect of the hole diameter (for the s ame vertical position) on fatigue crack growth rate, comparing plane strain and plane stress states. The dashed vertical lines represent the left and right limits of each hole. In both situations the effect of crack flank holes on fatigue crack growth is noticeable. Note that, for plane stress state, the plastic wake is under formation during the crack propagation, until a crack length of 15.5 mm, leading to a decrease in the evolution of the crack growth rate. Before the crack tip reaches the hole's position there is an increase of the fatigue crack growth rate, caused by the existence of the hole. On the other hand, the crack growth rate decreases once the crack crosses the hole position.

When the crack tip is far away from the centre of the hole, the hole effect must vanish, as the crack growth rate converges to the one obtained using the specimen without holes. Besides, the effect of the hole is stronger for larger diameters. Finally, results show that, under plane strain conditions, the hole has a higher effect when the crack is ahead of it, but in plane stress, the opposite is true.

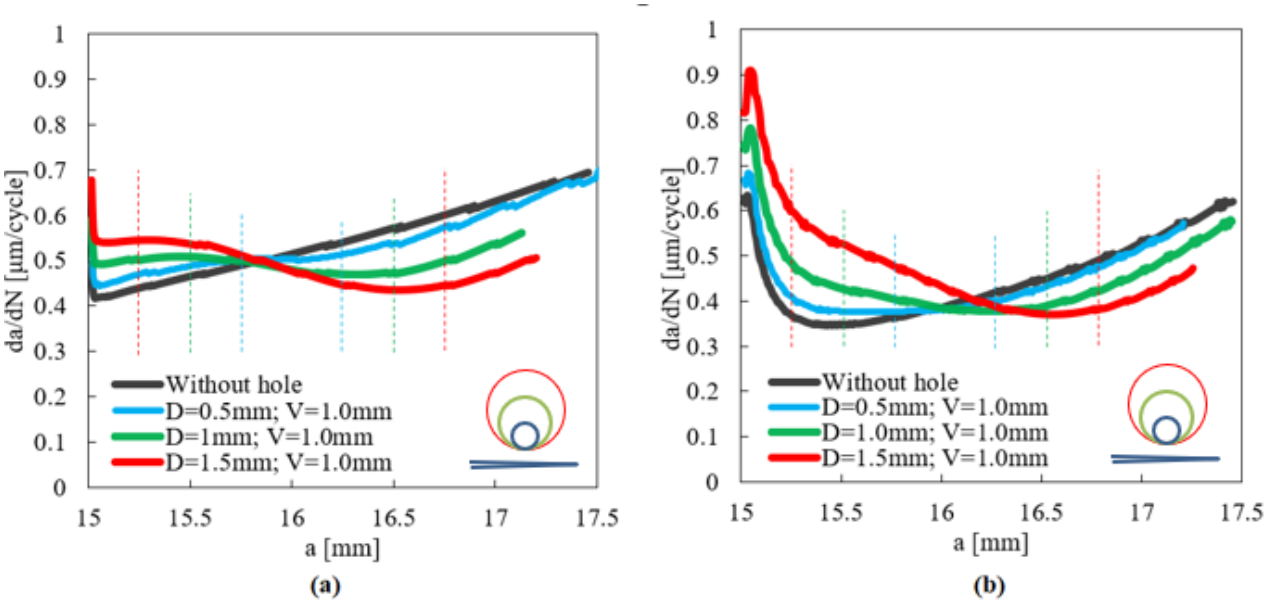

Figure 4.2. Effect of the hole diameter on FCG rate for the same vertical position: (a) plane strain state; (b) plane stress state.

Table 4.1 and Table 4.2 show the number of load cycles required to achieve both certain crack lengths and certain increments in crack length, respectively. Additionally, the Table 4.2 presents the difference between the load cycles required to fulfil each crack length increment.

Table 4.1. Number of load cycles to achieve each crack length.

	Plane Stress State			
	15.5mm	**16.0mm**	**16.5mm**	**17.0mm**
Without hole	1297	2689	3931	4981
D=0.5mm; V=1.0mm	1182	2539	3821	4902
D=1.0mm; V=1.0mm	1017	2273	3638	4846
D=1.5mm; V=1.0mm	831	1902	3219	4544

Table 4.2. Duration, in load cycles, of each crack length increment and the difference between these values.

	[15-16]mm	**[16-17] mm**	**Diff**
Without hole	2689	2292	-397
D=0.5mm; V=1.0mm	2539	2363	-176
D=1.0mm; V=1.0mm	2273	2573	300
D=1.5mm; V=1.0mm	1902	2642	740

The number of load cycles presented in Table 4.1 shows that the specimen with no holes requires more load cycles to reach the same crack length. However, in Table 4.2, the differences column shows that, a crack increase of 16 mm to 17 mm requires less load cycles in the case of the drilled specimens, relatively to the specimen with no hole. Additionally, the biggest difference is the one associated to the larger hole. This means that the presence of the hole is not beneficial in a first stage. However, if the hole is drilled in a position where the gain in load cycles is higher after the propagation starts, then the fatigue life of that component can be increased.

4.1.3. Effect of the hole's vertical position

Figure 4.3 presents the effect of two distinct vertical positions (V=1 mm and V=1.5mm), for the same hole diameter (D=1.5 mm), on the FCG. The case where no hole exists in the crack's vicinity is also presented. Note that, when the holes are located ahead of the crack tip, the effect of the holes is stronger under plane stress state. On the other hand, when the holes are located behind of the crack tip, the effect of the holes is stronger under plane strain conditions. Also, the FCG rate will converge to values corresponding to the specimen without holes when the crack tip is getting furthest away from the hole's centre. The effect of the holes is stronger when they are located closer to the crack. Indeed, the effect of the holes must disappear when they are located far away from the crack. The results show that, the FCG rate has the highest value for V=1 mm, until the crack reaches the centre of the hole (at a=16 mm). However, after this point, it becomes the lowest da/dN. Thus, FCG rate has the lowest value when the hole is positioned behind the crack tip (from 16 to 17 mm). For the case where the hole is positioned at a vertical position of 1.5 mm, the predicted FCG rate sits between the other situations, this is, without holes and V=1 mm.

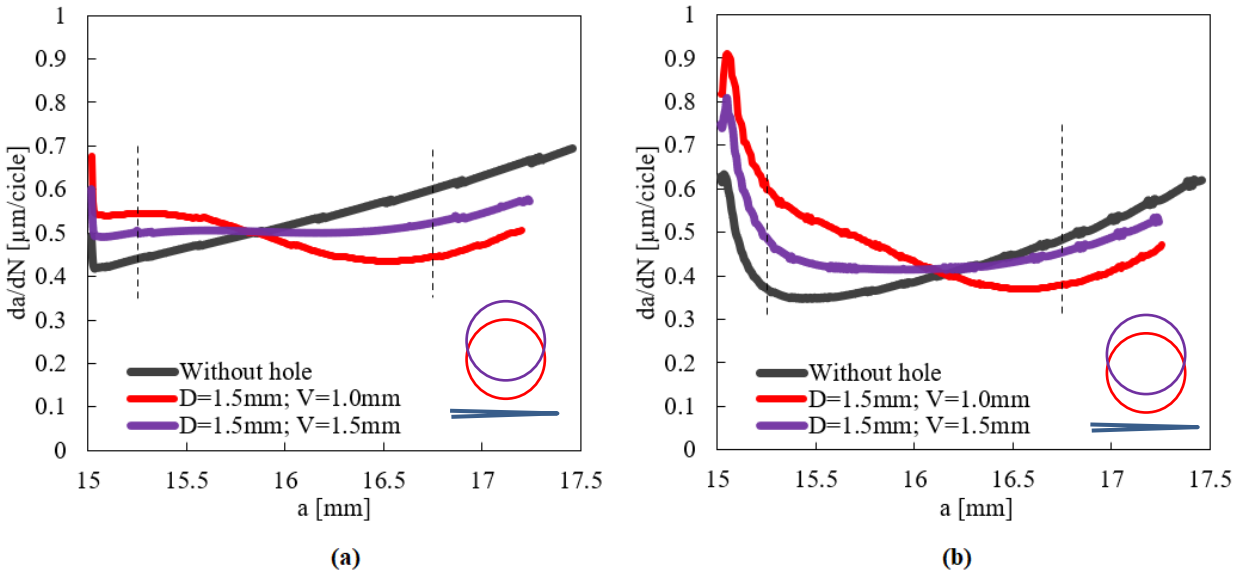

Figure 4.3. Effect of the vertical position on the fatigue crack growth rate for the same diameter: (a) plane strain state; (b) plane stress state.

4.1.4. Effect of contact between crack flanks

Figure 4.4 presents the effect of the contact between the crack flanks, on the evolution of FCG rate, in the specimen with holes of 1.5 mm in diameter and V=1 mm. To achieve this, cases with and without crack flanks contact, under plane strain and plane stress states, were studied. The results are compared with the ones obtained with a specimen without holes. Under plane strain, the contact between crack flanks has no significant effect on the FCG rate. Indeed, there is only a slight increase of the FCG rate for the specimen with a hole. On the other hand, for plane stress conditions the effect of contact between crack flanks is highly noticeable, since the *da/dN* values are much higher when the contact between the flanks is not taken into consideration. Additionally, in this case, the FCG rate is higher for the specimen with hole, but only before reaching 16 mm of crack length (coordinate of the centre of the hole), afterwards the largest *da/dN* occurs for the specimen without holes. Note, also, that the effect of the holes still exists without crack closure, which indicates that crack closure does not fully explain the geometrical effect.

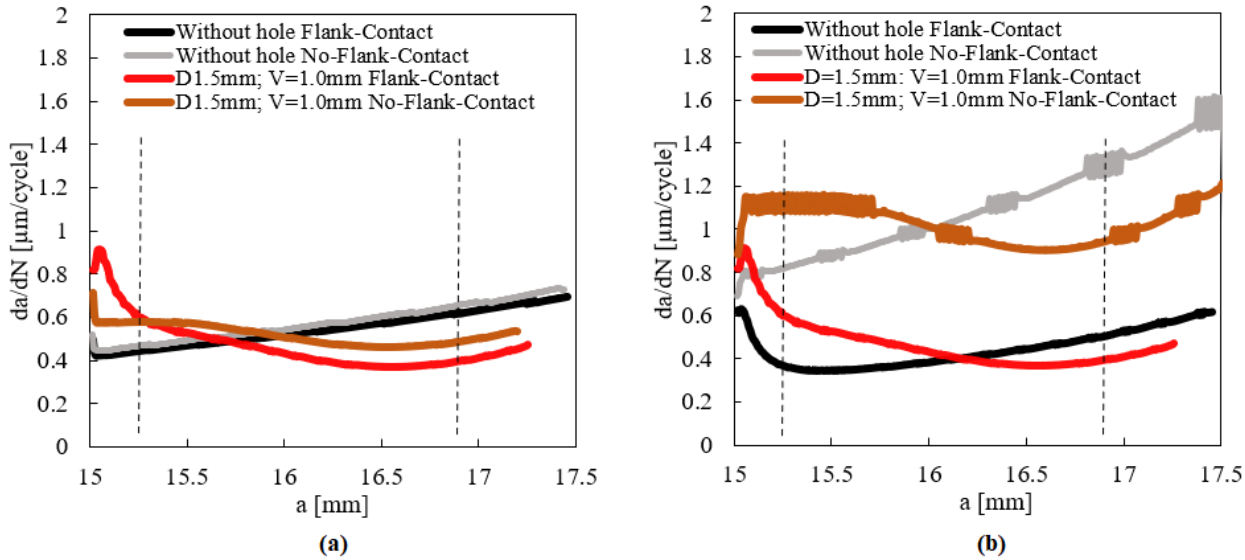

Figure 4.4. Effect of the contact of the crack flanks on the predicted fatigue crack growth rate in a specimen with holes of 1.5 mm diameter: (a) plane strain state; (b) plane stress state.

4.2. Crack tip opening displacement (CTOD)

The crack tip opening displacement was evaluated for the crack length of 17 mm and a hole vertical position, V=1 mm, comparing the different hole diameters. The results are shown for both plane strain and plane stress states.

4.2.1. Effect of the hole diameter

The effect of the hole diameter, on the CTOD, is shown in Figure 4.5. The results show that, regarding the fatigue crack growth rates (**Error! Reference source not found.**), lower v alues of CTOD are obtained for lower *da/dN* values. This behaviour is highly visible in plane strain state, particularly if one makes the CTOD curves coincident at the beginning, is easy to see that the blue curve would sit between the black and blue curves, in agreement with the *da/dN* results. For plane stress state (Figure 4.5b), although all curves have values relatively close to each other, the lowest values correspond to the 1.5 mm hole diameter, which arises the same for the *da/dN* values (**Error! Reference source not found.**b).

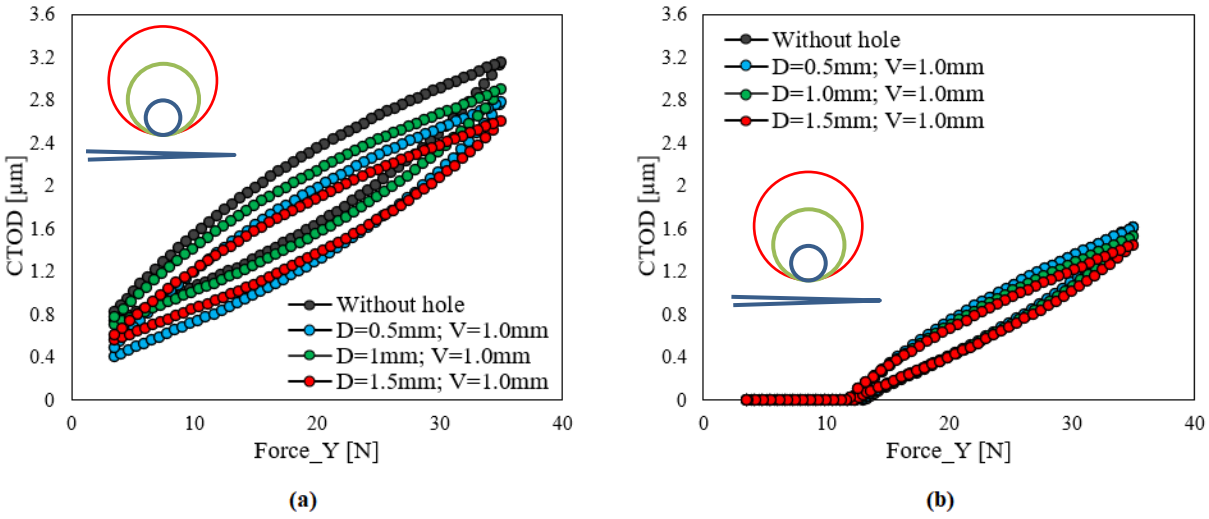

Figure 4.5. Effect of the hole diameter (same vertical position) on the crack tip opening displacement for a crack length of 17 mm: (a) plane strain state (b) plane stress state).

4.2.2. Effect of the hole's vertical position

In terms of the hole vertical position effect, results show that, under plane strain state (Figure 4.6a), the vertical placement of the hole has a more pronounced effect on CTOD when comparing to a plane stress state scenario (Figure 4.6b). In fact, the effect of vertical positioning is significantly less pronounced under plane stress conditions, where the crack closure is significant. The absence of crack closure was verified for all the simulations done for plane strain state. This is, for a crack length of 15.5 mm, 16.0 mm, 16.5 mm, and 17.0 mm, which allows us to conclude that crack closure has no impact on fatigue crack growth rates, for plane strain state. In plane stress state, however, crack closure was present in all the simulations done for the same crack lengths mentioned above, so it should have an impact on FCG.

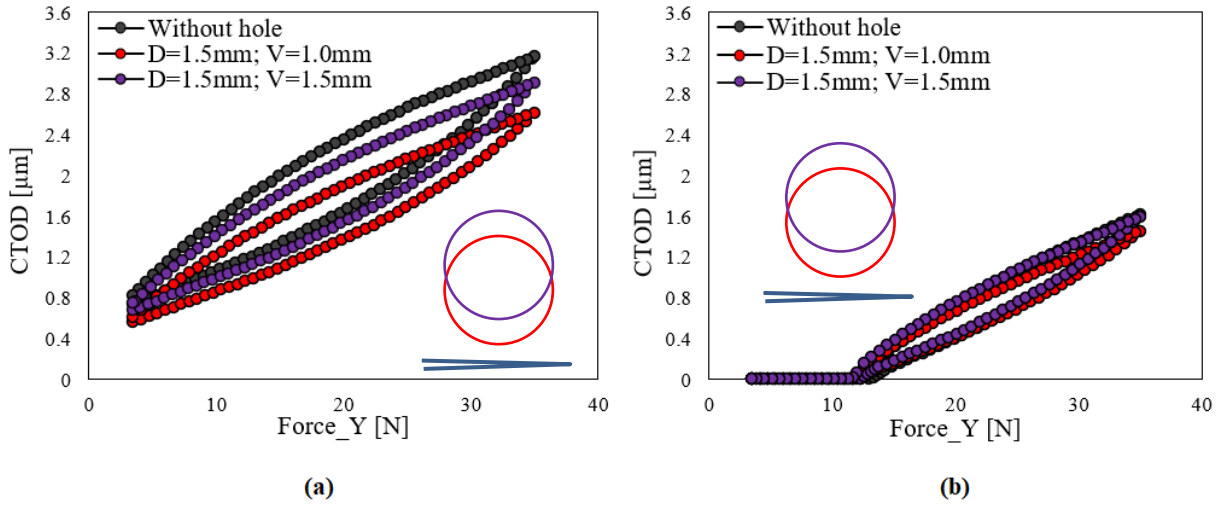

Figure 4.6. Effect of the vertical position of the holes on the crack tip opening displacement for a crack length of 17 mm: for the (a) plane strain state (b) plane stress state.

4.2.3. Effect of the contact between crack flanks

Figure 4.7 presents the effect of the contact between crack flanks, on the CTOD, for D=1.5 mm and V=1.0 mm. Results show no influence of the contact under plane strain state. This was expected because there is no crack closure even when the contact is considered. For plane stress state, there are negative CTOD values because the crack flanks are allowed to penetrate each other, which occurs at minimum load, as shown in Figure 4.8. The red region represents the overlapping region between the two crack flanks, which is physically impossible to achieve.

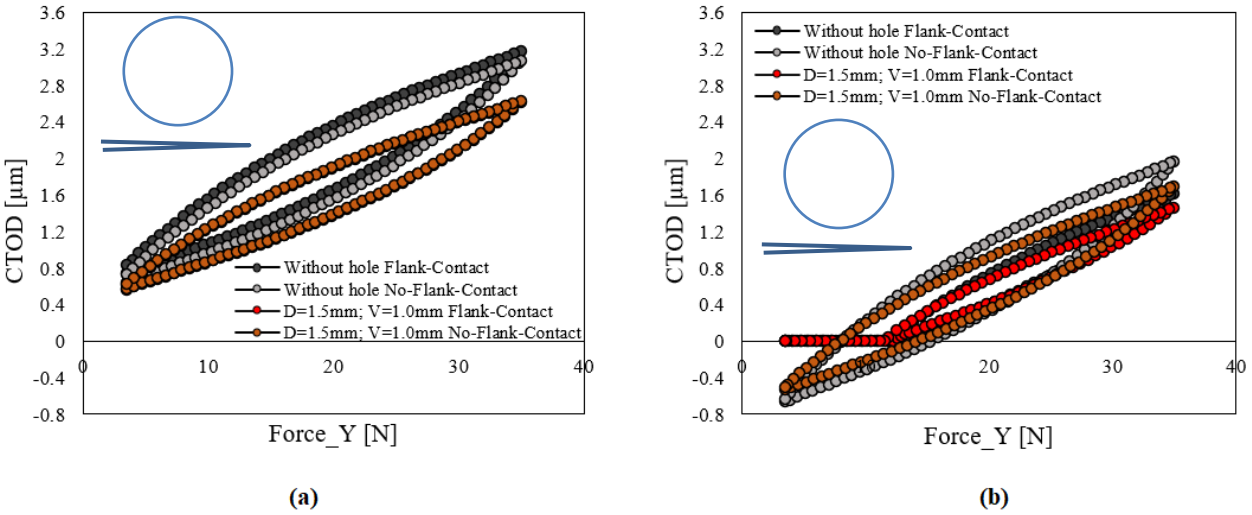

Figure 4.7. Effect of the contact between crack flanks on the crack tip opening displacement for a crack length of 17 mm and D=1.5 mm and V=1.0 mm: (a)plane strain state (b); plane stress state, CTOD.

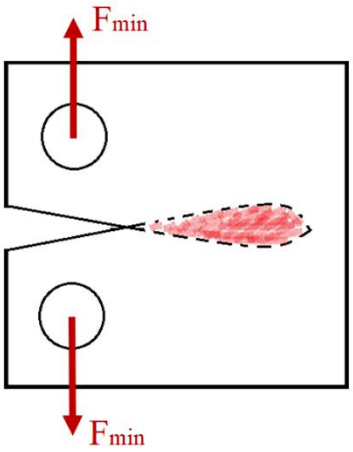

Figure 4.8. Crack closure example when contact between crack flanks is not considered.

4.3. Crack tip plastic strain

Figure 4.9 shows the effect of the hole diameter on the plastic strain evolution, at the crack tip, when the crack reaches a length of 17 mm. The horizontal axis represents the pseudo-time (represents the time interval starting when each specimen reached 17mm of crack length) to facilitate the comparison between different simulations. The specimen with the bigger hole, D=1.5 mm, has the lowest values of plastic strain at the beginning of each new propagation. Moreover, the plastic strain growth rate increases with the increase of the hole diameter. Therefore, the specimen with D=1.5 mm takes more load cycles to achieve the critical value of plastic strain. This confirms the obtained lower values of crack growth rate, for this diameter, presented in **Error! Reference source not found.**. The same can be s aid about the remaining geometries, i.e., the specimen with the highest FCG rate will take a shorter amount of time (load cycles) to reach the critical value of plastic strain, and vice-versa. Finally, the specimen with the smallest hole has a closer behaviour to the specimen without hole.

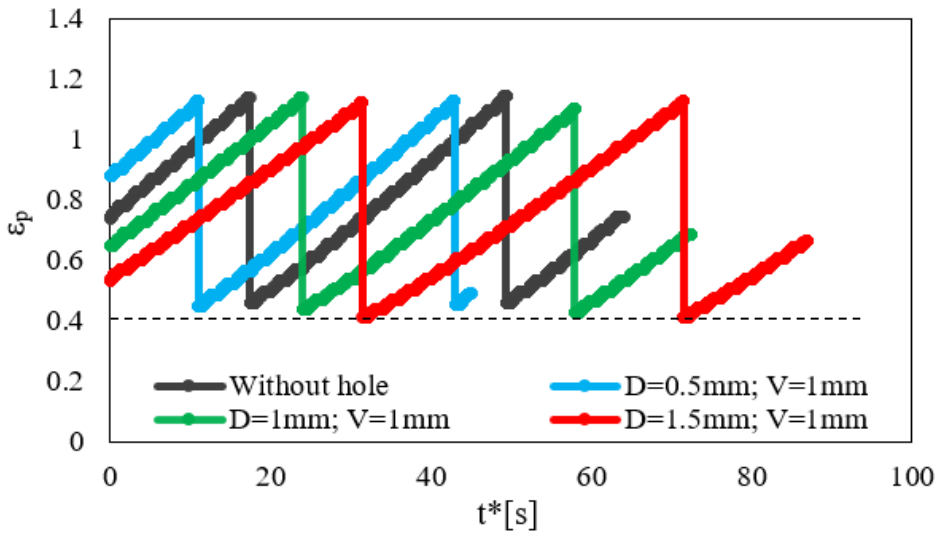

Figure 4.9. Influence of the hole diameter on the plastic strain evolution at the crack tip, for a crack length of 17 mm.

4.4. Equivalent plastic strain

Figure 4.10 shows the equivalent plastic strain distribution for the different hole diameters studied, for plane strain (a, b, c) and plane stress (d, e, f) states, considering a crack length of 17 mm. The highest levels of plastic strain occur along the crack path direction. Nevertheless, the plastic strain achieves values up to 0.5% closer to the edge of the hole. The non-uniform distribution along the hole periphery is related with the loading applied in the CT specimen, i.e., the cyclic load is applied in the left-side of the specimen and the crack is propagating towards to the right-side. The stress concentration around the crack tip is amplified when the hole is located ahead of the crack tip. On the other hand, when the hole is located behind the crack, the stress concentration around the crack tip is reduced. This effect is more pronounced has the size of the hole is increased. Therefore, drilling a hole behind the crack tip is the most beneficial position, to decrease further damage inflicted on the material.

For plane stress state, the effect is similar, being the plastic strain values higher behind the centre of the hole as its diameter increases. The biggest difference between plane stress and plane strain state is that, in plane stress state, the equivalent plastic strain has higher values ahead of the hole. Also, the equivalent plastic strain presented at the hole is more severe than for plane strain state. Also, the equivalent plastic strain presented at the hole is more severe than for plane strain state.

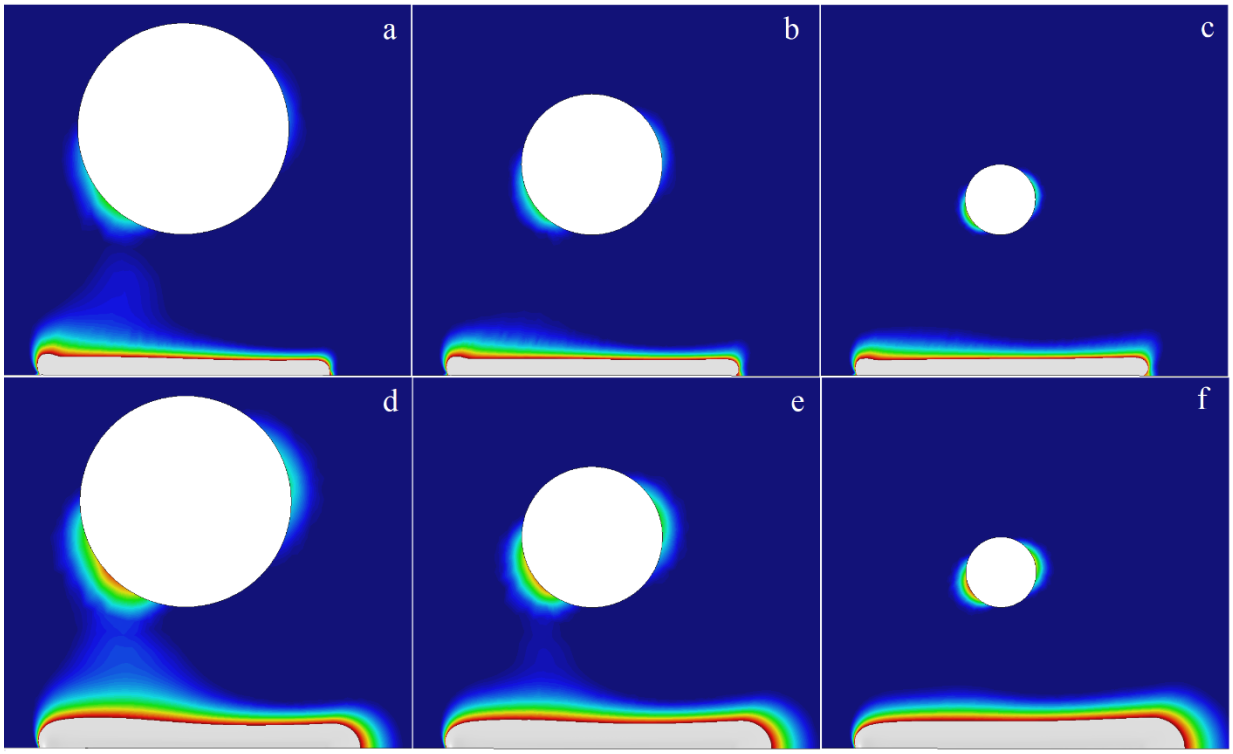

Figure 4.10. Effect of hole diameter in the equivalent plastic strain distribution, in plane strain (a, b, c) and plane stress (d, e, f) states and a crack length of 17 mm. a, d) D=1.5 mm; V=1.0 mm. b, e) D=1.0 mm, V=1.0 mm. c, f) D=0.5 mm; V=1.0 mm.

4.5. Crack closure

The evolution of the crack closure level, U*, during the crack propagation, predicted under plane stress state for different values of holes diameter is shown in Figure 4.11. As mentioned before, he dashed vertical lines represent the border of each hole while all of them are centred at a crack length corresponding to 16 mm.

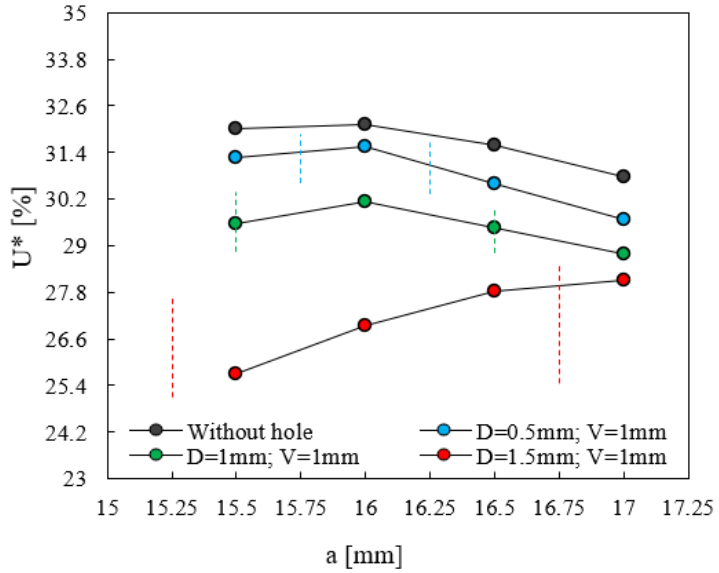

Figure 4.11. Evolution of the crack closure level (U*) during the crack propagation predicted under plane stress for different values of holes diameter (v=1,0mm).

The biggest hole (D=1.5 mm) shows a lower percentage of crack closure throughout the load cycles. However, this value increases as the crack crosses the hole. The holes with diameters of 1 mm and 0.5 mm show a different behaviour. Accordingly, the crack closure increases as the crack approaches the centre of the hole and decreases as it travels further away from this point. Between these two cases one found the specimen with the 1 mm hole, which shows a lower percentage of crack closure. Additionally, the crack closure is higher in the specimen that does not contain a hole. Therefore, the effect of the crack flank holes on the FGC rate is not directly related with the crack closure since it is always higher for the specimen without holes.

4.6. Stress field

The distribution of the vertical stress component, for plane stress state, at the instant of minimum load is presented in Figure 4.12, comparing the situation without hole and with a 1.5 mm diameter hole. Different crack lengths are analysed. In all cases, the stress is compressive immediately ahead of the crack tip, increasing as one moves away from this point until it achieves a maximum tensile value. The presence of the hole changes the stress field distribution, being this variation more noticeable while the crack is propagating through the hole.

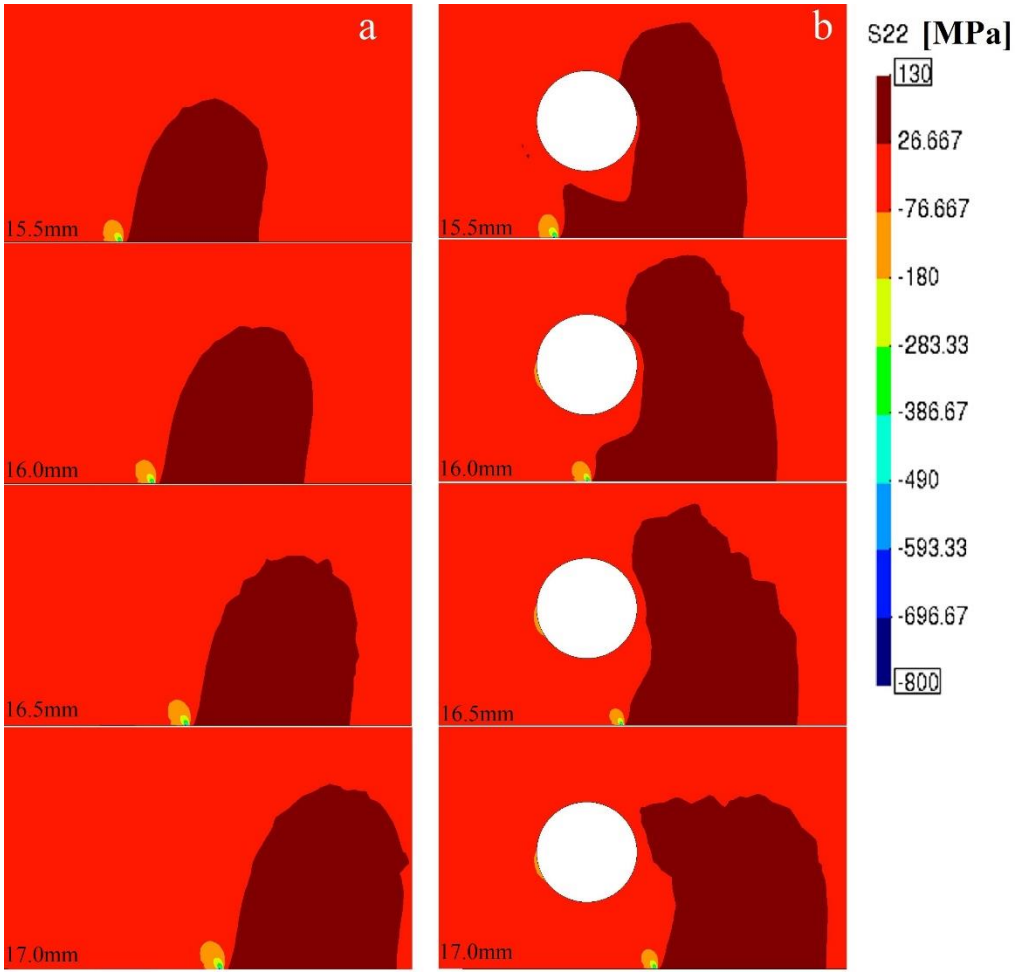

Figure 4.12. Vertical stress component field for the specimen with no hole (a) and a specimen with a 1.5 mm diameter hole (b), for plane stress state.

Figure 4.12a shows the expansion of the zone tensile stressed (darker zone), during the propagation of the crack. Results show that a larger area is being affected as the crack propagates due to the increase of the stress intensity factor range). For a crack length of 17 mm, the zone with the higher tensile stresses, in the specimen with hole, starts to appear like the same zone but for the situation without hole. This means that for a crack length higher than 17 mm the hole will no longer have a significant effect on FCG.

Figure 4.13 shows the vertical stress distribution (σ_Y) for the nodes ahead of the crack tip, when the crack length is of 17.0 mm. The crack tip is placed in x=0 mm, and "x" represents the distance to the crack tip. Results show that the diameter effect is not very significant and, after approximately 1.5 mm away from the tip, the hole has almost no effect on the stress distribution. The length ahead the crack tip, subjected to compressive stresses, is about 0.1 mm at the instant of minimum load.

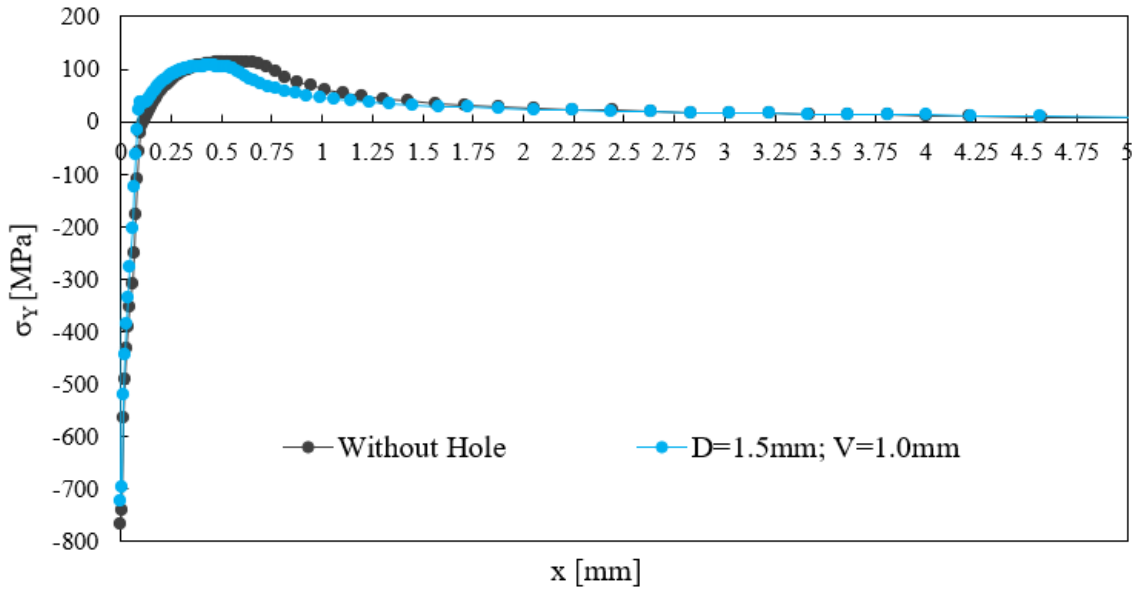

Figure 4.13. Stress distribution (y-axis) ahead of the crack tip, for plane stress state, and a crack length of 17 mm.

5. CASE STUDY

In order to validate the adopted numerical model and to check the accuracy of the numerical results, experimental trials are required. The information regarding the experimental procedure will be presented next, as well as the details of the numerical model under identical conditions of the experimental setup.

5.1. Material

Due to material availability, at the laboratory, trials are being performed for the AA2050-T8 aluminium alloy, which chemical composition is presented in Table 5.1. Regarding the mechanical proprieties, they were obtained for the S-T orientation (see Figure 5.1), which are listed in Table 5.2.

Table 5.1. Chemical composition for 2050-T8 aluminium alloy, in weight (%)

Al	Cu	Mg	Mn	Si	Fe	Zn	Li	Ag	Zr
Bal.	3.55	0.4	0.35	0.04	0.05	0.12	1	0.45	0.1

Table 5.2. Mechanical proprieties for the 2050-T8 aluminium alloy. Adapted from [58].

Orientation	**E [GPa]**	**υ**	**Y_0 [MPa]**	**C_X**	**X_{Sat} [MPa]**
S-T	70	0.33	316.87	416.88	19.8

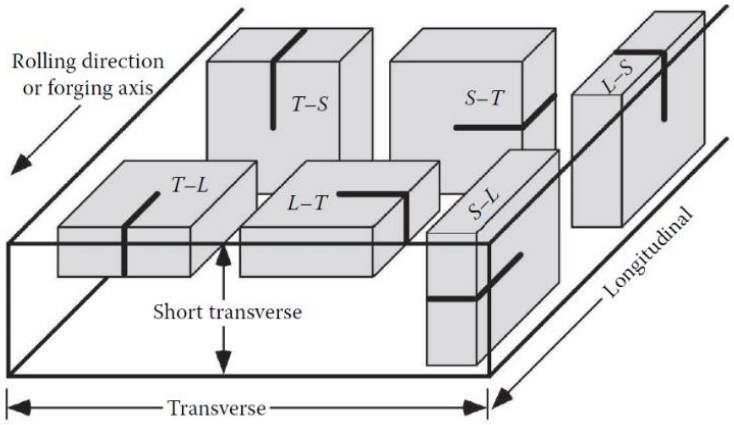

Figure 5.1. Orientation of the specimens. Adapted from [62]

The critical value of plastic strain required for the crack growth criterion (node release) must be calibrated for this material. This is achieved by comparing numerical and experimental *da/dN* results, for the same stress intensity factor range and stress ratio. The MT specimen with a=10 mm and R=0 was adopted to perform the comparison, adjusting the load to obtain 11.9 MPa(m)$^{0.5}$ of stress intensity factor range. The numerical values of crack growth rate were obtained for two different values of plastic strain (100% and 150%) using the same initial crack length of 9.9 mm. After linear interpolation, a value of $\Delta\varepsilon_{pc}$= 110% was obtained by comparing the precited FCG rate with the experimental value (0.00024 mm/cycle). Figure 5.5 shows the interpolation result and the obtained critical plastic strain value.

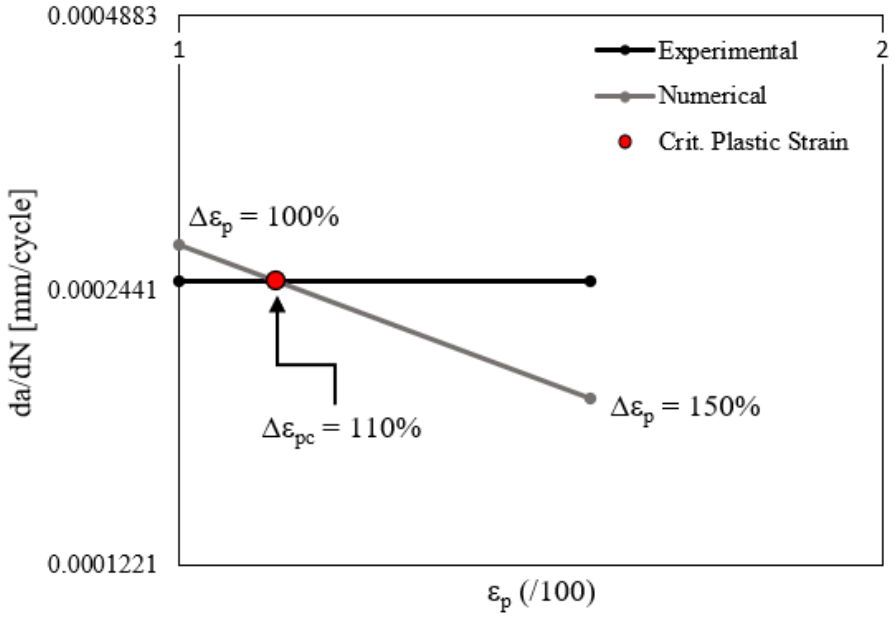

Figure 5.2. Critical plastic strain calibration process for the AA 2050-T8 alloy, for S-T orientation.

5.2. Specimen geometry

The new geometry of CT specimen used for direct comparison between numerical simulation and the experimental trials, with two pairs of drilled holes, is presented in Figure 5.3. The diameter chosen for the holes is consequence of the experimental limitations on drilling smaller holes. For each pair, a different load range is considered, since the value for ΔK must be approximately the same (identical to the value used in the previous numerical simulations). The distance between each hole in the pair had to be relatively large, to prevent a possible deviation of the crack path towards any of holes.

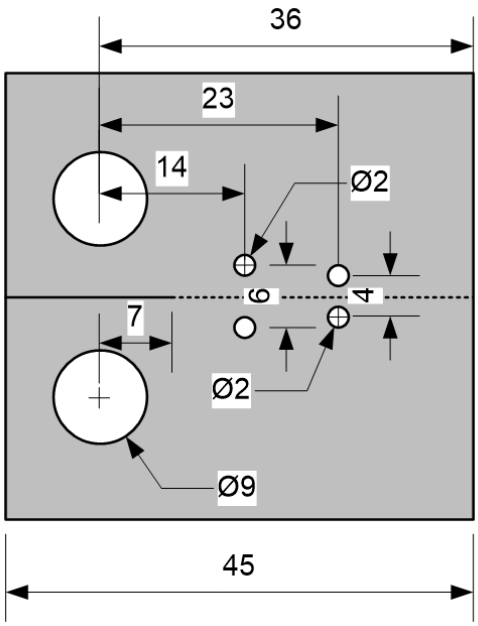

Figure 5.3. Specimen geometry used in the experimental approach.

5.3. Finite Element Mesh

In order to save time and computational resources, two different simulations were made, each one regarding one pair of holes with the respective load ranges and initial crack length. The finite element mesh used in the propagation between the first pair of holes is presented in Figure 5.4, where D=2 mm and V=2 mm. The finite element mesh used in the propagation between the second pair of holes is presented and Figure 5.5, where D=2 mm and V=1 mm. In both cases, the zone of refined mesh around the crack path comprises 6 mm of length. The meshes have the following characteristics:

- Element size in the zone where the crack will propagate: 0.008 mm (8 µm).
- Average element dimension in the crack vicinity: 0.2 mm
- Thickness: 0.1 mm

The finite elements are composed by linear hexahedral finite elements, and in total the meshes contain 51472 and 51524 elements, respectively.

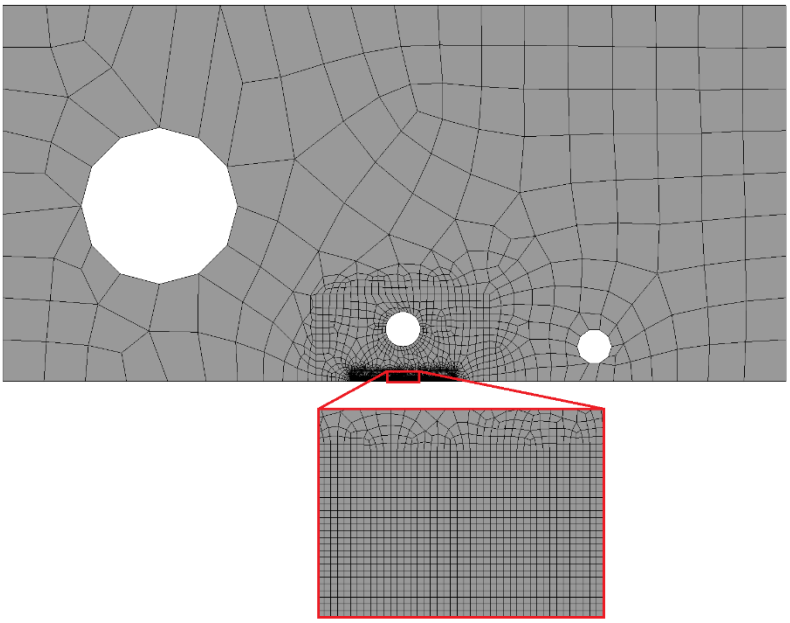

Figure 5.4. Finite element mesh corresponding to the first pair of holes (D=2mm, V=2mm).

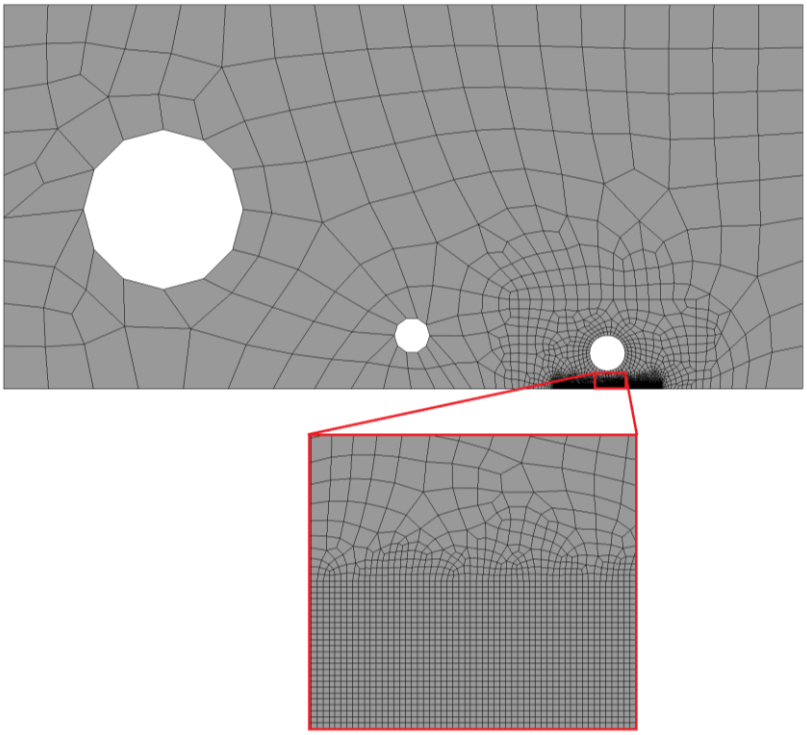

Figure 5.5. Finite element mesh corresponding to the second pair of holes (D=2mm, V=1mm).

5.4. Loading

Table 5.3 shows the maximum and minimum values for the applied force corresponding to each pair of holes. The load range for the first pair of holes is higher than the one for the second pair, to ensure the value of ΔK remains the same on both numerical simulations (around 13.7 MPa $m^{1/2}$) since the crack length is lower near the first pair of holes. For this CT specimen, with an initial crack length of 14 mm and using the load range listed in Table 5.3, one obtains a ΔK=13.75 MPa $m^{1/2}$. In the case where the initial crack length is 23 mm, ΔK=13.7 MPa $m^{1/2}$. The stress rate, R=0.1, is the same used for the previous simulations.

Experimental work is now underway.

Table 5.3. Load range for each geometry.

Holes	**a_0 [mm]**	**F_{max} [N]**	**F_{min} [N]**
D=2 mm; V=2 mm	14	41	4.1
D=2 mm, V=1 mm	23	18	1.8

6. CONCLUSIONS

The effect of crack flank holes on fatigue crack growth was evaluated using numerical simulation. Different hole diameters and positions were studied for the CT specimen, considering the aluminium alloy 2024-T351. The validation of the numerical model, with experimental results, is being carried out for the aluminium alloy 2050-T8.

For the 2024-T351 aluminium alloy, the results obtained throughout this thesis lead to the following conclusions:

- Effect of the hole presence.
  - The hole induces an increase on the FCG rates right from the start.
  - As the hole's influence fades, there is a rise on FCG rate until this value equals those for the situation with no hole.
- Effect of the hole diameter:
  - I. The predicted FCG rate increases with the hole diameter when the crack tip is behind the centre of the hole, and the opposite is verified after this point. This allow us to conclude that it is beneficial to have a larger hole behind the tip of the crack, in comparison with the other positions and diameters.
  - II. The overall number of cycles needed to achieve the final considered crack length is higher when no hole is drilled, indicating that having the hole from the start is not beneficial.
  - III. The CTOD values are lower for higher diameter holes, which sustains the results for *da/dN*.
  - IV. Specimens with larger holes show lower crack tip plastic strain values, at the beginning of each propagation. The plastic strain growth rate increases with the increase of the hole diameter.
  - V. The stress concentration around the crack tip is: i) amplified if the hole is ahead of the crack tip; ii) reduced if the hole is behind the crack tip. These results agree with the ones summarized in point I.
  - VI. The crack closure level decreases as the diameter of the hole increases. However, the specimen without holes shows higher levels of crack

closure than the drilled ones, which means the effect of crack flank holes on FCG rate is not directly related with the crack closure phenomenon.

- Effect of the hole vertical position:
  I. Holes have a stronger effect on fatigue crack growth rate when drilled closer to the crack path.
  II. Drilling holes closer to the crack will also result in lower CTOD values.
- Effect of contact between crack flanks:
  I. For plane strain conditions, the effect of the contact between crack flanks, in FCG rates, is not significant. However, under plane stress, the effect is highly noticeable.
  II. When contact between crack flanks is not considered, the fatigue crack growth rates are much higher (under plane stress conditions).
  III. The contact between crack flanks only has an influence in situations where crack closure is verified.

The present work indicates that the cumulative plastic strain may be used to study the effect of holes drilled near the crack flanks. It is beneficial for crack growth retardation to drill a larger hole, closer to the crack flanks, but only after crack propagation is verified, this is, at a certain instant of the fatigue life. Therefore, the solution that has higher chance of ceasing crack propagation is to drill a hole at the crack tip. An important conclusion is that crack closure does not directly explain the geometry effect on fatigue crack growth.

By the deadline for submission of this dissertation no numerical results for the 2050-T8 aluminium alloy were obtained, due to time availability and long simulation procedures. In a near future, the achievement of these results and final conclusions will be performed.

As suggestions for future work:

- Study the effects of holes including other mechanisms in the numerical analysis, namely using the GTN model which simulates the growth and coalescence of micro voids.
- Study the effect of other geometrical issues, namely make a comparison between CT and MT specimens using the cumulative plastic strain approach. Additionally, study the propagation of non-symmetrical cracks in MT specimens.

REFERENCES

[1] A. Silva Ribeiro, J. AFO Correia, A. S. Ribeiro, utadpt José AFO Correia, A. L. L Silva, and A. M. P de Jesus, "EVOLUTION OF FATIGUE HISTORY View project EVOLUTION OF FATIGUE HISTORY," 2010, Accessed: Mar. 24, 2022. [Online]. Available: https://www.researchgate.net/publication/299397997

[2] C. M. Branco, *Projeto de Sistemas Mecânicos*.

[3] E. Santecchia *et al.*, "A Review on Fatigue Life Prediction Methods for Metals," *Advances in Materials Science and Engineering*, vol. 2016. Hindawi Limited, 2016. doi: 10.1155/2016/9573524.

[4] C. Branco, *Mecânica dos Materiais*, 2nd ed.

[5] P. Paris, A. Director, and F. Erdogan, "A Critical Analysis of Crack Propagation Laws," 1963. [Online]. Available: http://fluidsengineering.asmedigitalcollection.asme.org/

[6] A. Trudel, "Recent trends in the design of hydropower components subjected to cycling and fatigue; towards improved technical design specifications," 2017, Accessed: Mar. 28, 2022. [Online]. Available: https://www.researchgate.net/publication/320310804_Recent_trends_in_the_design_of_hydropower_components_subjected_to_cycling_and_fatigue_towards_improved_technical_design_specifications

[7] T. K. G. Namboodhiri, " Crack growth behaviour in true corrosion fatigue," 2006.

[8] G. Lesiuk, "Application of a new, energy-based ΔS* crack driving force for fatigue crack growth rate description," *Materials (Basel).*, vol. 12, no. 3, Feb. 2019, doi: 10.3390/MA12030518.

[9] F. V Antunes, S. Serrano, R. Branco, and P. Prates, "Fatigue crack growth in the 2050-T8 aluminium alloy," 2018, doi: 10.1016/j.ijfatigue.2018.03.020.

[10] W. Elber, "Fatigue crack closure under cyclic tension," in *Eng. Fract. Mech.*, 1st ed., vol. 2, 1970, pp. 37–45.

[11] R. Pippan and A. Hohenwarter, "Fatigue crack closure: a review of the physical phenomena," *Fatigue Fract. Eng. Mater. Struct.*, vol. 40, no. 4, pp. 471–495, Apr. 2017, doi: 10.1111/FFE.12578.

[12] S. Suresh and C. M. Moss, “Near-Threshold Fatigue Crack Growth in 2 1 /iCr-1Mo Pressure Vessel Steel in Air and Hydrogen,” 1980, Accessed: Apr. 04, 2022. [Online]. Available: http://asme.org/terms

[13] S. Suresh and R. O. Ritchie, “On the Influence of Fatigue Underloads on Cyclic Crack Growth at Low Stress Intensities,” *Mater. Sci. Eng.*, vol. 51, pp. 61–69, 1981.

[14] S. Suresh and R. O. Ritchie, “A Geometric Model for Fatigue Crack Closure Induced by Fracture Surface Roughness”.

[15] A. G. Pineau and R. M. Pelloux, “Influence of Strain-Induced Martensitic Transformations on Fatigue Crack Growth Rates in Stainless Steels,” 1974.

[16] T. Ocawa’ and H. Kobayashi’, “NEAR-THRESHOLD FATIGUE CRACK GROWTH AND CRACK CLOSURE IN A NODULAR CAST IRON,” 1987.

[17] L. P. Borrego, J. M. Ferreira, and J. M. Costa, “Fatigue crack growth and crack closure in an AlMgSi alloy,” *Fatigue Fract. Eng. Mater. Struct.*, vol. 24, no. 4, pp. 255–265, 2001, doi: 10.1046/j.1460-2695.2001.00383.x.

[18] F. J. V. Antunes, “Fatigue Crack Growth in Metallic Materials,” no. April, 2021.

[19] J. Tong, “T-stress and its implications for crack growth,” *Eng. Fract. Mech.*, vol. 69, no. 12, pp. 1325–1337, 2002, doi: 10.1016/S0013-7944(02)00002-4.

[20] C. J. Christopher, M. N. James, E. A. Patterson, and K. F. Tee, “Towards a new model of crack tip stress fields,” *Int. J. Fract.*, vol. 148, no. 4, pp. 361–371, 2007, doi: 10.1007/s10704-008-9209-3.

[21] C. J. Christopher, M. N. James, E. A. Patterson, and K. F. Tee, “A quantitative evaluation of fatigue crack shielding forces using photoelasticity,” *Eng. Fract. Mech.*, vol. 75, no. 14, pp. 4190–4199, 2008, doi: 10.1016/j.engfracmech.2008.03.013.

[22] M. F. Borges, D. M. Neto, and F. V. Antunes, “Numerical simulation of fatigue crack growth based on accumulated plastic strain,” *Theor. Appl. Fract. Mech.*, vol. 108, p. 102676, 2020, doi: 10.1016/j.tafmec.2020.102676.

[23] N. A. Fleck, “Finite element analysis of plasticity-induced crack closure under plane strain conditions,” *Eng. Fract. Mech.*, vol. 25, no. 4, pp. 441–449, 1986, doi: 10.1016/0013-7944(86)90258-4.

[24] R. C. McClung, B. H. Thacker, and S. Roy, “Finite element visualization of fatigue crack closure in plane stress and plane strain,” *Int. J. Fract.*, vol. 50, no. 1, pp. 27–

49, 1991, doi: 10.1007/BF00035167.

[25] J. Wu and F. Ellyin, “A study of fatigue crack closure by elastic-plastic finite element analysis for constant-amplitude loading,” *Int. J. Fract.*, vol. 82, no. 1, pp. 43–65, 1990, doi: 10.1007/BF00017863.

[26] L. G. Zhao, J. Tong, and J. Byrne, “The evolution of the stress-strain fields near a fatigue crack tip and plasticity-induced crack closure revisited,” *Fatigue Fract. Eng. Mater. Struct.*, vol. 27, no. 1, pp. 19–29, 2004, doi: 10.1111/j.1460-2695.2004.00716.x.

[27] H. Alizadeh *et al.*, “A comparison of two and three-dimensional analyses of fatigue crack closure,” *Int. J. Fatigue*, vol. 29, no. 2, pp. 222–231, 2007, doi: 10.1016/j.ijfatigue.2006.03.014.

[28] N. A. Fleck and J. C. Newman, “Analysis of crack closure under plain strain conditions,” 1986.

[29] J. D. M. Costa and J. A. M. Ferreira, “Effect of stress ratio and specimen thickness on fatigue crack growth of CK45 steel,” *Theor. Appl. Fract. Mech.*, vol. 30, no. 1, pp. 65–73, 1998, doi: 10.1016/S0167-8442(98)00044-5.

[30] W. Guo, C. H. Wang, and L. R. F. Rose, “Influence of cross-sectional thickness on fatigue crack growth,” *Fatigue Fract. Eng. Mater. Struct.*, vol. 22, no. 5, pp. 437–444, 1999, doi: 10.1046/j.1460-2695.1999.00176.x.

[31] P. Hutař, S. Seitl, and Z. Knésl, “Quantification of the effect of specimen geometry on the fatigue crack growth response by two-parameter fracture mechanics,” *Mater. Sci. Eng. A*, vol. 387–389, no. 1-2 SPEC. ISS., pp. 491–494, 2004, doi: 10.1016/j.msea.2004.05.043.

[32] M. R. Ayatollahi, S. M. J. Razavi, and H. R. Chamani, “A numerical study on the effect of symmetric crack flank holes on fatigue life extension of a SENT specimen,” *Fatigue Fract. Eng. Mater. Struct.*, vol. 37, no. 10, pp. 1153–1164, 2014, doi: 10.1111/ffe.12199.

[33] K. H, T. S, and I. K, “NEW METHOD OF ARRESTING FATIGUE CRACK GROWTH BY ARTIFICIAL WEDGE.,” in *Advances in Colloid and Interface Science*, 1979, pp. 282–293.

[34] W. Yanyan, Z. Mingxu, and F. Daqing, “a Study of Retarding Fatigue Crack Growth Using an Artificial Wedge,” *Fatigue Fract. Eng. Mater. Struct.*, vol. 16, no.

3, pp. 363–376, 1993, doi: 10.1111/j.1460-2695.1993.tb00093.x.

[35] P. K. Sharp and G. Clark, “Retardation and repair of fatigue cracks by adhesive infiltration,” vol. 20, no. 4, pp. 605–614, 1997.

[36] M. R. Ayatollahi and R. Hashemi, “Mixed mode fracture in an inclined center crack repaired by composite patching,” *Compos. Struct.*, vol. 81, no. 2, pp. 264–273, 2007, doi: 10.1016/j.compstruct.2006.08.013.

[37] C. Zhang, S. van der Vyver, X. Hu, and P. Lu, “Fatigue crack growth behavior in weld-repaired high-strength low-alloy steel,” *Eng. Fract. Mech.*, vol. 78, no. 9, pp. 1862–1875, 2011, doi: 10.1016/j.engfracmech.2011.03.004.

[38] R. L. Carlson, G. A. Kardomateas, and P. R. Bates, “The effects of overloads in fatigue crack growth,” *Int. J. Fatigue*, vol. 13, no. 6, pp. 453–460, 1991, doi: 10.1016/0142-1123(91)90479-I.

[39] P. S. Song and G. L. Sheu, “Retardation of fatigue crack propagation by indentation technique,” *Int. J. Press. Vessel. Pip.*, vol. 79, no. 11, pp. 725–733, 2002, doi: 10.1016/S0308-0161(02)00096-0.

[40] A. H. Fairand, B. P. and Clauer, “Effect of water and paint coatings on the magnitude of laser-generated shocks,” vol. 18, no. 4, pp. 0–3, 1976.

[41] J. M. Yang, Y. C. Her, N. Han, and A. Clauer, “Laser shock peening on fatigue behavior of 2024-T3 Al alloy with fastener holes and stopholes,” *Mater. Sci. Eng. A*, vol. 298, no. 1–2, pp. 296–299, 2001, doi: 10.1016/S0921-5093(00)01277-6.

[42] S. Wang, Y. Li, M. Yao, and R. Wang, “Compressive residual stress introduced by shot peening,” *J. Mater. Process. Technol.*, vol. 73, no. 1–3, pp. 64–73, 1998, doi: 10.1016/S0924-0136(97)00213-6.

[43] P. K. Ray, B. B. Verma, and P. K. Mohanthy, “Spot heating induced fatigue crack growth retardation,” *Int. J. Press. Vessel. Pip.*, vol. 79, no. 5, pp. 373–376, 2002, doi: 10.1016/S0308-0161(02)00019-4.

[44] P. S. Song and Y. L. Shieh, “Stop drilling procedure for fatigue life improvement,” *Int. J. Fatigue*, vol. 26, no. 12, pp. 1333–1339, 2004, doi: 10.1016/j.ijfatigue.2004.04.009.

[45] R. Ghfiri, A. Amrouche, A. Imad, and G. Mesmacque, “Fatigue life estimation after crack repair in 6005 A-T6 aluminum alloy using the cold expansion hole technique,” *Fatigue Fract. Eng. Mater. Struct.*, vol. 23, no. 11, pp. 911–916, 2000,

doi: 10.1046/j.1460-2695.2000.00356.x.

[46] C. Makabe, A. Murdani, K. Kuniyoshi, Y. Irei, and A. Saimoto, “Crack-growth arrest by redirecting crack growth by drilling stop holes and inserting pins into them,” *Eng. Fail. Anal.*, vol. 16, no. 1, pp. 475–483, 2009, doi: 10.1016/j.engfailanal.2008.06.009.

[47] C. S. Shin, C. M. Wang, and P. S. Song, “Fatigue damage repair: A comparison of some possible methods,” *Int. J. Fatigue*, vol. 18, no. 8, pp. 535–546, 1996, doi: 10.1016/S0142-1123(96)00029-1.

[48] A. Murdani, C. Makabe, A. Saimoto, and R. Kondou, “A crack-growth arresting technique in aluminum alloy,” *Eng. Fail. Anal.*, vol. 15, no. 4, pp. 302–310, 2008, doi: 10.1016/j.engfailanal.2007.02.005.

[49] M. R. Ayatollahi, S. M. J. Razavi, C. Sommitsch, and C. Moser, “Fatigue life extension by crack repair using double stop-hole technique,” *Mater. Sci. Forum*, vol. 879, pp. 3–8, 2017, doi: 10.4028/www.scientific.net/MSF.879.3.

[50] H. Chen, W. Chen, T. Li, and J. Ure, “Effect of circular holes on the ratchet limit and crack tip plastic strain range in a centre cracked plate,” *Eng. Fract. Mech.*, vol. 78, no. 11, pp. 2310–2324, 2011, doi: 10.1016/j.engfracmech.2011.05.004.

[51] H. Tresca, “Memoir on the flow of solid bodies under strong pressure,” *Comptes Rendus l’Académie Sci. Paris*, vol. 59, pp. 754–758, 1864.

[52] R. V. von Mises, “Mechanik der festen korper im plastic-deformablen zustand. Nachrichten vos der koniglichen gellesschaft des winssenschaften zu Gottingen,” in *Math. klasse*, 1913, pp. 582–592.

[53] R. Hill, “The Mathematical Theory of Plasticity.” 1950.

[54] P. Prates, “Inverse Methodologies,” no. September, 2014.

[55] E. Voce, “The relationship between stress and strain for homogeneous deformation,” *J. Inst. Met.*, vol. 74, pp. 537–652, 1948.

[56] H. W. Swift, “Plastic instability under plane stress,” *J. Mech. Phys. Solids*, vol. 1, no. 1, pp. 1–18, 1952, doi: 10.1016/0022-5096(52)90002-1.

[57] J. Lemaitre and J.-L. Chaboche, *Mechanics of solid materials*. 1990.

[58] J. S. Jesus, F. V Antunes, P. Prates, R. Branco, P. V Antunes, and L. P. Borrego, “Influence of specimen orientation on fatigue crack growth in 7050-T7451 and 2050-T8 aluminium alloys,” pp. 1–22, 2022.

[59] L. S. Lasdon, A. D. Warren, A. Jain, and M. W. Ratner, “Design and testing of a Generalized Reduced Gradient Code for Nonlinear Optimization,” Cleveland, 1975.

[60] B. Moreno, “Fatigue crack propagation under random loading,” 2002.

[61] M. C. Oliveira, J. L. Alves, and L. F. Menezes, “Algorithms and strategies for treatment of large deformation frictional contact in the numerical simulation of deep drawing process,” *Arch. Comput. Methods Eng.*, vol. 15, no. 2, pp. 113–162, 2008, doi: 10.1007/s11831-008-9018-x.

[62] T. L. Anderson, *Fracture Mechanics: Fundamentals and Applications, Fourth Edition*, vol. 76. 2017.